Voltage tunes mGlu 5 receptor function, impacting synaptic transmission

Marin Boutonnet, Camille Carpena, Nathalie Bouquier, Yan Chastagnier, Joan Font-Ingles, Enora Moutin, Ludovic Tricoire, Jean Chemin, Julie Perroy

Voltage tunes mGlu5 receptor function, impacting synaptic transmission

Marin Boutonnet[1], Camille Carpena[1], Nathalie Bouquier[1], Yan Chastagnier[1], Joan Font-Ingles[1,2], Enora Moutin[1], Ludovic Tricoire[3], Jean Chemin[1], Julie Perroy[1]*

[1]IGF, University of Montpellier, CNRS, INSERM, Montpellier, France.

[2]Present address: SpliceBio, Barcelona, Spain.

[3]Neuroscience Paris Seine, Institut de biologie Paris Seine, Sorbonne universite, CNRS, INSERM, Paris, France

*Corresponding author: julie.perroy@igf.cnrs.fr

Short title: Voltage-dependent control of synaptic transmission by GPCRs

Key words: G-Protein Coupled Receptors (GPCR), metabotropic glutamate receptor (mGlu5), voltage sensitivity, signaling, biosensors, synaptic transmission, neuronal plasticity

Data Availability Statement - The data that support the findings of this study are available from the corresponding author upon reasonable request. Some data may not be made available because of privacy or ethical restrictions.

Bulleted point summary

What is already known:

- Some of the GPCRs are voltage-sensitive.

What this study adds:

- mGlu5 activation and signaling are optimal at resting membrane potential of neurons.

- mGlu5 primes NMDA receptor activation at the resting potential of neurons

Clinical significance:

- mGlu5 and/or NMDA receptors involvement in inducing plasticity may depend on recent neuronal activity

- mGlu5 voltage-sensitivity may play a critical role in pathologies associated with variations in intrinsic excitability

Abstract

Background and Purpose

Voltage sensitivity is a common feature of many membrane proteins, including some G-protein coupled receptors (GPCRs). However, the functional consequences of voltage sensitivity in GPCRs are not well understood.

Experimental approach

In this study, we investigated the voltage sensitivity of the post-synaptic metabotropic glutamate receptor mGlu5 and its impact on synaptic transmission. Using biosensors and electrophysiological recordings in non-excitable HEK293T cells or neurons.

Key Results

We found that mGlu5 receptor function is optimal at resting membrane potentials. We observed that membrane depolarization significantly reduced mGlu5 receptor activation, Gq-PLC/PKC stimulation, Ca^{2+} release, and mGlu5 receptor-gated currents through TRPC6 channels or NMDA receptors. Notably, we report a previously unknown activity of the NMDA receptor at the resting potential of neurons, enabled by mGlu5.

Conclusions & Implications

Our findings suggest that mGlu5 receptor activity is directly regulated by membrane voltage which may have a significant impact on synaptic processes and pathophysiological functions.

Introduction

G-protein coupled receptors (GPCRs) are 7-transmembrane receptors involved in numerous physiological processes and remain the most extensively targeted protein family by approved drugs (Lagerström and Schiöth, 2008). Recent research has unveiled that the activity of certain GPCRs can be modulated by the membrane voltage (V_m), about thirty out of the thousand members of this big family, including acetylcholine (Ben-Chaim et al., 2003, 2006; Navarro-Polanco et al., 2011; Rinne et al., 2015), purine (Martinez-Pinna et al., 2005), opioid (Ruland et al., 2020), dopamine (Sahlholm et al., 2008), and prostanoid receptors (Kurz et al., 2020). In neurons, where V_m undergoes permanent changes, this emerging property could significantly impact the functioning of neurotransmitter-activated GPCRs and their role as modulators of synaptic transmission. Although the structural mechanisms that underlie the sensitivity of GPCRs to V_m are still being elucidated (Ohana et al., 2006; Rinne et al., 2015; Barchad-Avitzur et al., 2016; Hoppe et al., 2018; López-Serrano et al., 2020), functional studies using site-directed mutagenesis of the V_m sensor suggest that GPCR activity can be affected, leading to impaired neurotransmitter release (Kupchik et al., 2011; Zhang et al., 2020) or synaptic plasticity and behavior (Rozenfeld et al., 2021).

Glutamate is the primary excitatory neurotransmitter in the brain that binds to both ionotropic (AMPA, NMDA, Kainate receptors) and metabotropic glutamate (mGlu) receptors. The mGlu receptor family, comprising eight G protein-coupled receptors (mGlu1-8), has been extensively studied for their modulatory role in synaptic transmission and plasticity (Scheefhals and MacGillavry, 2018). Preclinical and clinical studies have targeted these receptors in various neurological disorders, such as Autism, Fragile X syndrom, Schizophrenia, Parkinson's, and Alzheimer's disease (Niswender and Conn, 2010). So far, only one study, in

the Xenopus oocytes expression system, suggests a direct sensitivity of some mGlu receptors to V_m (mGlu1 and 3, (Ohana et al., 2006)). Yet, due to their synaptic location, these receptors are permanently exposed to membrane voltage fluctuations. Therefore, demonstrating the sensitivity of mGlu receptors to V_m could provide insights into their role depending on the state of neuronal activity. In this study, we have selected the postsynaptic mGlu5 receptor as a model receptor, known for its role as neuromodulator of synaptic transmission. mGlu5 is also a key trigger in the induction of synaptic plasticity, working in concert with ionotropic NMDA receptors through physical and functional crosstalk (Reiner and Levitz, 2018). Interestingly, NMDA receptors are a prototype of receptors whose activity is regulated by the membrane potential. As a detector of neuronal activity coincidence, NMDA activation is limited to synapses whose pre- and postsynaptic elements are activated simultaneously (Seeburg et al., 1995; Kwag and Paulsen, 2012). Thus, a sensitivity of the mGlu5 receptor to V_m could similarly specify the identity of synapses on which mGlu5 exerts its functional effects depending on the neuron's activity history.

In this report, using a variety of biosensors and patch clamp recordings, we explore and investigate the impact of V_m on the intricate signaling pathways associated with the conformational change of postsynaptic mGlu5 receptor induced by glutamate binding. This conformational change leads to the activation of $G_{q/11}$-type proteins, the activation of the PLC-PKC pathway, and the subsequent release of Ca^{2+} from internal stores through IP3 receptors (Niswender and Conn, 2010), ultimately fine-tuning synaptic transmission by gating channels and ionotropic receptors, including NMDA (Aniksztejn et al., 1992; Mannaioni et al., 2001; O'neill et al., 2018), AMPA (Hu et al., 2010; Holz et al., 2019), and transient receptor potential canonical (TRPC) channels (Lepannetier et al., 2018). Our data reveals that the mGlu5 receptor functions optimally at voltage close to the resting potential of the cells.

Results

V_m regulates mGlu5-induced Ca^{2+} release

To investigate the effect of V_m on mGlu5 function and determine the optimal experimental conditions, we examined mGlu5-induced Ca^{2+} release from intracellular stores. mGlu5 stimulation is known to induce a transient increase of Ca^{2+} oscillations in various cell types, including cultured astrocytes (Nakahara et al., 1997), hippocampal neurons (Rae et al., 2000), midbrain neurons (O'Malley et al., 2003), as well as in heterologous expression systems such as Chinese Hamster Ovary cells (Nash et al., 2002) and Human Embryonic Kidney 293T (HEK293T) cells (Gómez-Santacana et al., 2017). In line with these findings, in HEK293T cells expressing the GCaMP6s fluorescent Ca^{2+} sensor (**Figure 1A**), mGlu5 agonist (RS)-3,5-dihydroxyphenylglycine (DHPG, 100 µM) induced a Ca^{2+} increase exclusively in cells expressing mGlu5, as evidenced by GCaMP6s fluorescence fluctuations measured in the cell population using a fluorimeter (**Figure 1B**). The mGlu5 agonist-induced Ca^{2+} increase in mGlu5-expressing cells was inhibited by application of MPEP (10 µM), a mGlu5-specific negative allosteric modulator (NAM), confirming the requirement of mGlu5 receptor activation (**Figure 1B**).

In order to determine the effect of V_m on mGlu5-induced Ca^{2+} increase, we treated cells with equimolar solutions containing increasing concentrations of KCl (from 3 mM, a physiological concentration referred to as "V_{rest}", up to 100 mM) to induce a systematic, well-controlled,

and long-lasting membrane depolarization (as previously demonstrated in neurons (Moutin et al., 2021)). Interestingly, KCl 100 mM had no effect on basal intracellular Ca^{2+} concentrations (**Figure Supp. 1A**), but significantly reduced mGlu5 agonist-induced Ca^{2+} increase by 22.3 ± 7.1% compared to KCl 3 mM (**Figure 1C**). We measured that KCl 100 mM application increased the membrane potential by 23.6 ± 0.9 mV (**Figure 1D**), referred to as "V_{depol}". Whole cell patch clamp recordings indeed reported a reversible switch from V_{rest} = -28.4 ± 3.5 mV at physiological KCl concentration (3 mM) to V_{depol} = -4.8 ± 0.9 mV with KCl 100 mM (**Figure 1D**). The dose response curve of DHPG-induced Ca^{2+} release further revealed a reduction of the agonist efficacy at V_{depol} compared to V_{rest} (**Figure 1E**). Additionally, saturating concentrations of another mGlu5 agonist, quisqualate (10µM), triggered a Ca^{2+} increase at V_{rest}, which was reduced by 45 ± 9.5% at V_{depol} (**Figure 1F**). These initial findings indicate that the ability of the mGlu5 receptor to increase intracellular Ca^{2+} is dependent on V_m. To investigate whether the effect of V_m was specific to the mGlu5 receptor, we examined another G_q-coupled receptor, the angiotensin II type 1 receptor (AT1), and did not observe any influence of V_m on AT1 receptor-mediated Ca^{2+} release, thereby supporting a specific effect of V_{depol} on mGlu5 signaling in this context (**Figure 1G**).

To investigate the effect of V_m on mGlu5-induced Ca^{2+} increase at a cellular level, we performed live cell imaging of GCaMP6s fluorescence (**Figure 2A** and **supplemental Video1**). Initially, large recordings in the entire field of view showed a global increase in Ca^{2+} induced by the mGlu5 agonist, quisqualate (10µM), at V_{rest}. This increase was significantly reduced at V_{depol} (30 ± 10 % reduction compared to V_{rest} at the peak of fluorescence, **Figure 2B** and **supplemental Video2**). The global Ca^{2+} increase was an average of the single cell Ca^{2+} fluctuations, which were classified into 3 distinct populations of cells depending on the type of responses: silent cells, cells displaying 1 single Ca^{2+} spike, and Ca^{2+} oscillating cells (**Figure**

2C), as reported previously (Bradley et al., 2009, 2011). V_{depol} modified the distribution of cells in each of these categories, with a global shift towards less oscillating populations (**Figure 2C**), and a significant reduction in the proportion of cells with an oscillating Ca^{2+} pattern (10.6% reduction of the proportion of oscillating cells compared to V_{rest}, **Figure 2D**). Subsequently, for each oscillating cell, we studied the global frequency of Ca^{2+} oscillations induced by mGlu5 agonist. Quisqualate induced a mean of 0.49 ± 0.02 oscillations/min per cell at V_{rest}, but only 0.39 ± 0.02 oscillations per cell at V_{depol}. Thus, V_{depol} induced a 20.3 ± 4.8% reduction in the frequency of Ca^{2+} oscillations triggered by mGlu5 stimulation (**Figure 2E**).

Given that depolarization in neurons can also occur following receptor stimulation, we investigated the impact of V_{depol} subsequent to mGlu5 activation. Specifically, we measured the effect of V_{depol} compared to V_{rest} on oscillating cells that had undergone Ca^{2+} oscillations at resting membrane potential as a result of mGlu5 stimulation. To do so, we determined the instantaneous frequency, which represents the average inter-oscillation frequency between the first and last oscillations. Our findings consistently revealed a significant reduction in the instantaneous frequency, from 1.18 ± 0.11 at V_{rest} to 0.85 ± 0.04 oscillation/min at V_{depol}, representing a 28 ± 4.7% decrease (**Figure 2F**). These results suggest that a membrane depolarization of approximately 20-25mV, whether it occurs before or after mGlu5 activation, can diminish the receptor's ability to induce Ca^{2+} release from intracellular stores, in few seconds. Specifically, V_{depol} reduced the number of agonist-responsive cells and the efficiency of the responding cells, resembling the characteristics of a NAM (Bradley et al., 2009, 2011).

V_m tunes mGlu5 receptor probability of activation

The reduced ability of mGlu5 receptor to induce Ca^{2+} release from intracellular stores at V_{depol} may be attributed to a decrease in the expression of receptors at the plasma membrane and/or a diminished activation of these receptors under depolarized conditions. To investigate the first hypothesis, we measured the receptor cell surface expression using an enhance bystander Bioluminescence Resonance Energy Transfer (ebBRET) biosensor. ebBRET is based on naturally interacting chromophores luciferase (RLuc) and green fluorescent protein (rGFP) from *Renilla reniformis*, enabling to quantify the cell surface expression of an Rluc-tagged protein expressed with the rGFP anchored at the plasma membrane by a CAAX sequence ((Namkung et al., 2016) **Figure Supp. 2A**). In mGlu5-RlucII and rGFP-CAAX co-transfected cells, incubation of MPEP for 5 to 30 minutes resulted in an expected increase in receptor expression at the cell surface, as reported by an increase in ebBRET (**Figure Supp. 2B**). This control experiment validated the use of the ebBRET biosensor. However, we did not observe any ebBRET variation induced by shorter (2 min) applications of MPEP or quisqualate, nor by V_{depol} alone or combined with these ligands (**Figure Supp. 2C**). Therefore, this experiment ruled out any potential effect of V_{depol} on the receptor cell surface expression, in these experimental conditions.

To investigate the proportion of active and inactive mGlu5 receptors at the cell surface, we then used a Time-Resolved Fluorescence Resonance Energy Transfer (TR-FRET) biosensor, reporting structural dynamics and drug action at the mGlu5 receptor (Doumazane et al., 2013; Scholler et al., 2017). The conformational changes of the extracellular ligand-binding domains (ECDs) of mGlu5 dimers are associated with receptor activation: SNAP-mGlu5 (ST-mGlu5) labeled with the Lumi4-Tb donor and the fluorescein acceptor, display a high FRET signal in the absence of ligand or in presence of the antagonist and a low FRET signal in the presence of glutamate or other orthosteric agonists (**Figure 3A**). Any approach expected to stabilize the

active conformation of the effector domain increases the agonist potency in stabilizing the active ECDs conformation (Doumazane et al., 2013). Hence, TR-FRET measurements allowed to determine the proportion of active and inactive ST-mGlu5 receptors, depending on V_m. Importantly, labelling mGlu5 receptors separately on distinct cell populations, we first controlled that neither the fluorescein nor the Lumi4-Tb emissions were affected by V_{depol} (**Figure Supp 1B**), ruling out any effect of V_{depol} on the performance of the biosensor. In ST-mGlu5 expressing cells co-labeled with Lumi4-Tb and fluorescein (**Figure 3B**), quisqualate (10µM) induced a decrease in TR-FRET at V_{rest} (-17.2 ± 4.7%), reporting an agonist-induced increase of mGlu5 receptors in an active-like conformation. However, TR-FRET intensities measured in presence of quisqualate were significantly increased at V_{depol} (+7.0 ± 2.6%) compared to V_{rest}, indicating that V_{depol} reduced the ability of the agonist to trigger conformational activation of the receptor (**Figure 3B**). This lower efficiency of quisqualate at V_{depol} to decrease the TR-FRET reports a higher proportion of mGlu5 receptors in an inactive-like conformation at V_{depol} compared to V_{rest}. Consistently, we noticed a shift in IC_{50} of the LY341495 mGlu competitive antagonist, from 31.28 µM at V_{rest} to 6.75 µM at V_{depol} (**Figure 3C**), demonstrating a V_m effect on ligand affinity for the mGlu5 receptor orthosteric pocket. These results demonstrate the influence of V_m on the conformation of the receptor. V_{depol} stabilizes the inactive-like conformation of the receptor, increasing the antagonist potency.

V_m modulates mGlu5-mediated $G_{q/11}$ activation

We then assessed the influence of V_m on the activation by mGlu5 receptor of canonical effectors, starting with the $G_{q/11}$ activation. We monitored $G_{q/11}$ activation by mGlu5 using Effector Membrane Translocation Assay (EMTA) ebBRET (Avet et al., 2022) in single-cell BRET

imaging ((Goyet et al., 2016), **Figure 4**) and cell population (**Figure Supp. 3**). HEK293T cells were transfected with mGlu5, $G_{q/11}$, p63hRhoGEF-RlucII and rGFP-CAAX coding plasmids. $G_{q/11}$ activation triggers the recruitment of its cytosolic effector, p63RhoGEF-RlucII, to the plasma membrane, which is reported by an increase in ebBRET with the plasma membrane-anchored rGFP-CAAX. The ebBRET signal is therefore a measure of $G_{q/11}$ activation ((Avet et al., 2022), **Figure 4A**). Of note, the ebBRET signal was not affected by V_{depol} compared to V_{rest}, validating the use of this biosensor to assess the influence of V_m on mGlu5-induced $G_{q/11}$ activation (**Figure Supp 1C**). Application of DHPG (100µM) induced a slight but significant increase in ebBRET at V_{rest} and V_{depol} (**Figure 4B** and **4C**). Paired measurement of the DHPG net effect from individual cell ebBRET values revealed a mean DHPG-induced increase of 97 ± 9.9 milliBRET units at V_{rest}, and only 22.8 ± 6.2 at V_{depol} (**Figure 4D**). These findings indicate a significant reduction of mGlu5 receptor-induced $G_{q/11}$ activation at V_{depol}. Similar results were obtained with ebBRET measurement in cell populations, where the mGlu5 agonist-induced increase of ebBRET was significantly reduced by V_{depol} (agonist-induced ebBRET increase was reduced by 24.8 ± 7.2 % at V_{depol} compared to Vrest, **Figure Supp 3A**). The same protocol applied to AT1 receptor showed no influence of V_m on AT1 receptor agonist-induced $G_{q/11}$-coupling (**Figure Supp 3B**), suggesting once again that V_{depol} specifically affects mGlu5 receptor signaling.

V_m affects mGlu5 gating of TRPC6 channels

Transient Receptor Potential Channels (TRPC) are well known effectors of GPCRs intracellular secondary messengers. Typically, TRPC6 opening is triggered by the PLC signaling cascade that triggers formation of diacylglycerol (DAG) and inositol 1,4,5-trisphosphate (IP3, (Hof et al., 2019)). In particular, mGlu5 receptor induces TRPC6-dependent Ca^{2+} influx (Nagy et al., 2013;

Wang et al., 2019). We then further tested the influence of V_m on the ability of mGlu5 to gate TRPC6 channels. For this purpose, we co-transfected mGlu5-Venus and TRPC6-tomato in HEK293T cells and recorded whole-cell currents induced by DHPG (100µM), in voltage-clamp experiments (**Figure 5)**. In cells co-expressing mGlu5 and TRPC6 (**Figure 5B**), but not in cells expressing mGlu5 alone (**Figure 5A**), DHPG applied at a holding potential of -80mV triggered a large inward current with similar kinetics and amplitude than previously reported in HEK293T cells (Itsuki et al., 2014). The current-voltage relationship (I/V curve, **Figure 5C**) also displayed typical TRPC6 permeation and rectification properties (Dryer and Kim, 2018). Given that the ions flow through open channels is governed by the membrane potential, we could not simply compare the current density generated and recorded by activation of mGlu5 at different potentials. We therefore perfused the mGlu5 agonist at different holding potentials (either -80 mV or -20 mV) and then rapidly recorded the currents generated over the full range of V_m ramping (from -80mV to +60mV in 100ms, **Figure 5C**). When DHPG was applied at a holding potential of -20mV instead of -80 mV, the current amplitude recorded with the same voltage ramp protocol was strongly reduced. For example, we recorded a mean inward current density of 46.65 ± 10.32 pA/pF at -80 mV triggered by DHPG application at -80mV, versus 17.69 ± 6.36 pA/pF at -80 mV when DHPG was applied at -20mV (**top insert, Figure 5C**). Importantly, these two protocols triggered the same I/V curve in non-stimulated cells, excluding a holding potential-dependent artefact during the recordings (**Figure Supp 4**). These results confirm that mGlu5 is more active at resting potentials compared to depolarized potentials, which impacts TRPC6 gating by mGlu5 downstream effectors.

V_m regulates mGlu5-induced Ca^{2+} release in hippocampal neurons

We further investigated whether mGlu5 voltage-sensitivity also controls its function in neurons. We therefore first studied the ability of mGlu5 receptors to induce calcium release from intracellular stores in hippocampal neurons depending on the membrane potential. To address this, we systematically inhibited other sources of calcium fluctuations in neurons, including voltage-dependent calcium channels (100 µM Nickel and 100 µM Cadmium), ionotropic glutamate receptors of the AMPA (10 µM NBQX) and NMDA (50 µM AP5) types, and metabotropic receptors of the mGlu1 type (100 µM CPCCOEt). Neurons were incubated in a medium containing 3 mM (V_{rest}) or 55 mM KCl (V_{depol}, which depolarizes neurons from -70 mV to –30 mV (Moutin et al., 2021)) and GCaMP6s fluorescence fluctuations were recorded before and after mGlu5 receptor stimulation with DHPG (50 µM). Activation of mGlu5 receptors resulted in calcium transients that diffused throughout the neuron and recurred at a regular frequency (**Figure 6 and Supplementary Videos 3 and 4**). The number of events induced by DHPG was reduced at V_{depol} compared to V_{rest} (**Figure 6A and C**), along with a decrease in the number of oscillations per neuron (**Figure 6A and B**). These neuronal findings closely parallel those obtained in HEK cells (described in **Figures 1 and 2**), confirming the responsiveness of mGlu5 receptors to membrane potential and the optimal release of calcium from intracellular stores at the resting potential of neurons.

V_m regulates mGlu5-NMDA receptors crosstalk in hippocampal neurons

The NMDA receptor conductance is well established to be regulated by type I mGlu receptors (Lutzu and Castillo, 2021). Specifically, NMDA receptor potentiation by mGlu5 receptors involves the G_q-protein-coupled receptor (GPCR) pathway, which includes protein kinase C (PKC) and Src signaling, in various neuronal contexts (Anikstejn et al., 1992; Pisani et al., 1997;

Mannaioni et al., 2001; Benquet et al., 2002; Heidinger et al., 2002; O'neill et al., 2018). We investigated whether V_m could regulate the crosstalk between mGlu5 and NMDA receptors in primary cell cultures of hippocampal neurons (**Figure 7**). To avoid stimulation of mGlu1 receptors, we used the mGlu1-specific negative allosteric modulator (NAM), CPCCOEt (100 µM), while stimulating mGlu5 receptors with DHPG. We recorded NMDA-induced currents in the absence of magnesium (Mg^{2+}) to prevent voltage-dependent blockade of NMDA receptors. When applied alone at a holding potential of -80 mV, DHPG (50 µM) had a negligible effect (1.046 ± 0.45 pA/pF). In contrast, NMDA (30 µM) induced an inward current of 23.4 ± 3.7 pA/pF (**Figure 7A**), which was potentiated by 39.5 ± 6.5% by DHPG when applied at -80 mV ($I_{NMDA + DHPG}/I_{NMDA}$ ratio measured just before and after DHPG application, **Figure 7B, 7C left**). However, at a holding potential of -40 mV, DHPG only induced a 25.4 ± 5.2% potentiation of NMDA current density (**Figure 7B, 7C right**). Paired measurements of $I_{NMDA + DHPG}/I_{NMDA}$ performed subsequently at -80 mV or -40 mV on the same neuron in a random order confirmed a reduction of DHPG-induced NMDA receptor potentiation at -40 mV (+25 ± 4.8%) compared to -80 mV (+38.11 ± 8.2%) (**Figure 7D**). These results demonstrate the crucial role of V_m in the control of mGlu5-NMDA crosstalk in neurons, and they corroborate our previous findings on the global voltage-dependence of mGlu5 receptor activity, which is inhibited by depolarized membrane potentials.

Therefore, the optimal functioning of the mGlu5 receptor, which enhances NMDA receptor activity in neurons, occurs at the resting potential of neurons. This finding appears to conflict with the fact that NMDA receptors are typically blocked by Mg^{2+} at resting membrane potential. Activation of the NMDA receptor indeed requires depolarization of the postsynaptic element to release Mg^{2+} from the channel pore, and simultaneous binding of glutamate released from the depolarized axon terminal. However, recent studies have shown that the

physiological concentration of Mg^{2+} in the interstitial medium (0.7 mM, (Ding et al., 2016)) is lower than what is typically used experimentally in the ACSF composition to record ex vivo neuronal activity, suggesting that the NMDA receptor activity at resting potential in physiological concentrations of Mg^{2+} may have been underestimated (Chiu and Carter, 2022). Furthermore, GluN2D-containing receptors may exhibit reduced Mg^{2+} sensitivity compared to GluN2A- or GluN2B-containing receptors (Sobczyk et al., 2005). Therefore, to resolve the physiological relevance of optimal potentiation of NMDA receptors by mGlu5 at a potential at which NMDA receptors are predominantly inactive, we investigated the mGlu5-induced potentiation of NMDA receptors at resting potential in the presence of 0.7 mM Mg^{2+}, by recording currents and calcium transients (**Figure 8**). Whole-cell current recordings revealed a residual NMDA-induced current of 1.80 $\pm$ 0.30 pA/pF density, which was potentiated to 2.40 $\pm$ 0.40 pA/pF by DHPG co-application (**Figure 8A**). The full current potential relationships are displayed in **Figure 8B**. In a second set of experiments, we measured calcium fluctuations, still in presence of physiological concentrations of Mg^{2+} at resting potential, before and after DHPG application, followed by application of AP5 at the end of the experiment to identify NMDA-dependent events (**Figure 8C and Suppl Video 5**). GCaMP6s fluorescence fluctuations highlighted basal spontaneous Ca^{2+} transients of various shape, size, and kinetics, as illustrated by a projection of all spontaneous Ca^{2+} transients recorded during 2 min and 15 sec (**Figure 8C$_1$**). The variety of these Ca^{2+} events certainly relies on the nature of the receptors, channels and intracellular stores involved in their triggering. DHPG increased the number of calcium transients (**Figure 8D**) and their area under curve (AUC) significantly increased from 0.102 $\pm$ 0.001 to 0.154 $\pm$ 0.002 following DHPG application (**Figure 8E**). The majority of events were blocked by AP5 (50 µM) at the end of the experiment, revealing NMDA-dependent events (**Figure 8C$_4$ and 8D**). To further focus on the effect of DHPG on NMDA-dependent events, we

first filtered and selected small and non-propagating calcium transients (which are properties expected from NMDA-dependent synaptic events in a spine-confined environment, **Figure 8C$_{2-4}$**), and further identified *a posteriori* regions of interest (ROIs) that were extinguished by AP5 on **Figure 8C$_4$** because the events previously recorded in these areas (**Figure 8C$_{2-3}$**) depended on NMDA receptors. Interestingly, DHPG changed the shape of the NMDA-dependent events, inducing a more sustained calcium inflow over time (**Figure 8F**). Taken together, our data show that the mGlu5 receptor potentiates NMDA receptor activity at resting membrane potential, increasing currents and particularly calcium influx, thus expanding the functional importance of NMDA receptors to resting neurons.

Discussion

The mGlu5 receptor functions optimally at the resting potential of cells.

In this study, we demonstrate that the activity and signaling of the mGlu5 receptor is influenced by the membrane potential of the cell, highlighting an aspect of the receptor that has previously been overlooked. Specifically, a depolarization of the membrane promotes an inactive-like conformation of the receptor, a reduction in mGlu5 coupling to $G_{q/11}$ and subsequent release of Ca^{2+} from intracellular stores. This results in a reduced activation of downstream effectors, including TRPC6 channels and ionotropic NMDA receptors. In the exact same experimental conditions, no effect of V_m was observed on activation of the AT1 receptor, which however activates the same pathway as the mGlu5 receptor (Rössig et al., 1996; García-

Sáinz et al., 1997; Inuzuka et al., 2016), highlighting the specificity of V_m action on mGlu5 receptor signaling. The mGlu5 receptor is a critical component in the modulation of synaptic transmission, and it plays a role in both inducing and regulating Hebbian and homeostatic synaptic plasticity processes. As such, the sensitivity of the mGlu5 receptor to membrane potential will impact its functions, and its role may vary depending on the context of neuronal activity.

The mGlu5 receptor senses moderate V_m variations, similar to natural fluctuations of membrane potential occurring at synapses.

A modest increase in membrane potential by approximately 20-25 mV is sufficient to reduce mGlu5 receptor activity by half. Our findings reveal that the mGlu5 receptor is highly sensitive to changes in membrane potential compared to other GPCRs which require stronger depolarizations, at least twice the level used in our study, and sometimes up to 140 mV, to induce a similar shift in receptor efficacy (Navarro-Polanco et al., 2013; Birk et al., 2015; Rinne et al., 2015). Both patch clamp and KCl depolarization methods resulted in the same polarity of membrane potential effect on mGlu5 receptor function. Moreover, the effect of depolarization was comparable when applied before or during agonist perfusion, suggesting that membrane potential can either prevent optimal activation or rapidly reverse ongoing activation of the mGlu5 receptor. Notably, changes in dendritic spine membrane potential during post-synaptic potentials have been reported to be in the range of 20-25 mV, a magnitude similar to that observed in our study (Acker et al., 2016; Jayant et al., 2017; Cornejo et al., 2022). Thus, local synaptic potentials may mediate rapid modulation of mGlu5 function in neurons. Although membrane potential changes were applied tonically in our study, similar

results have been obtained by others using physiological frequency ranges, mimicking trains of action potentials (Hoppe et al., 2018; Zhang et al., 2020). A more resolutive investigation would provide better insights into the intensity and duration of membrane potential variations required to modulate mGlu5 receptor activity and refine our understanding of the type of neuronal activity of similar magnitude and temporal order that could affect mGlu5 function.

Membrane depolarization controls mGlu5 receptor activity, as a NAM.

The scope of this study did not include the identification of the voltage sensor within the mGlu5 receptor. However, previous studies on other GPCRs have identified molecular determinants of V_m sensitivity, such as the binding sites of orthosteric or allosteric ligands, G protein binding domains, or Na^+ ions within the 7TM (David et al., 2022). These studies mainly concern class A GPCRs, where the molecular sites mentioned above are located in the 7TM. Unfortunately, very little is known about the voltage-sensing domains of class C GPCRs, to which the mGlu5 receptor belongs. Nevertheless, it is reasonable to assume that the voltage sensor is also located in the 7TM, directly exposed to the magnetic field. This hypothesis is supported by structural studies showing that activation of the 7TM stabilize the active conformation of the extracellular domains of the mGlu5 receptor (Nasrallah et al., 2021). In the atypical structure of class C GPCRs, the extracellular domains of the receptor (and the orthosteric binding site) are approximately 10 nm distant from the membrane (Nasrallah et al., 2021), out of the membrane electric field, which excludes their involvement as a voltage sensor. In contrast, allosteric modulators bind to the 7TM of the receptor. Interestingly, many studies show that V_m affects the efficiency or agonist potency of class A GPCRs in a manner

similar to allosteric modulators (Navarro-Polanco et al., 2013; Birk et al., 2015; Hoppe et al., 2018). Specifically, tyrosine residues located in the allosteric site are involved in V_m detection by GPCRs (Barchad-Avitzur et al., 2016). Of note, the allosteric binding site of the mGlu5 receptor also contains a tyrosine residue (Tyr6593.44) that enables NAM inhibitory effects (Mølck et al., 2012; Nasrallah et al., 2021).

Functional data collected in this study suggests that membrane depolarization causes a NAM effect on the mGlu5 receptor. Indeed, NAMs cause a decrease in agonist efficacy with virtually no changes on agonist potency (Niswender and Conn, 2010), similar to the effect of depolarization on the dose-response curve (**Figure 1E**). Furthermore, mGlu5 receptor-mediated Ca^{2+} oscillations are known to undergo frequency reduction by NAMs, such as MPEP, supported by a decrease in the proportion of oscillating cells (Bradley et al., 2009, 2011). Interestingly, a similar process is induced by membrane depolarization, namely, a reduction in frequency when depolarization is applied before or after the initiation of oscillations, correlated with a decrease in the proportion of oscillating cells (**Figure 2 and 6**).

Reconsideration of mGlu5 and NMDA functions

Our study suggests that the optimal functioning of mGlu5 receptors at resting membrane potential may potentiate NMDA receptors too. Traditionally, NMDA receptors are known to be “coincidence detectors” of pre- and post-synaptic activation because they are blocked by the Mg^{2+} ion at resting potential (SEEBURG et al., 1995; Kwag and Paulsen, 2012). However, our results indicate that they may also play an unexpected role at resting potential, facilitated by the permissive effect of mGlu5 receptors. Our findings add complexity to the functional cross-talk between mGlu5 and NMDA receptors, with mGlu5 priming NMDA receptor

activation on recently resting neurons. Once the membrane potential is depolarized enough to unblock NMDA receptors, they can function autonomously, while negative feedback from V_m on mGlu5 receptors limits NMDA facilitation and synapse overexcitability. This finding is likely to have significant implications for the nature of induced neuronal plasticity, which relies on the concerted activities of mGlu5 and NMDA receptors (Francesconi et al., 2004; Neyman and Manahan-Vaughan, 2008). Different cellular mechanisms for inducing plasticity will come into play depending on the type of activatable receptor following network activity.

The acute effect of depolarization on the activity and signaling of mGlu5 receptors adds to the extensive regulation of protein complexes around these receptors and their functional interactions that are regulated by neuronal activity. The mGlu5 receptor has been proposed as a homeostatic regulator of synaptic transmission, a role that requires activity-induced monomeric Homer1a expression (Hu et al., 2010; Diering et al., 2017; Bockaert et al., 2021). Within the neuronal environment, the function of mGlu5 receptors is dynamically regulated by interactions with multimeric Homer proteins, which is dampened by the monomeric Homer1a protein during sustained synaptic activity (Ango et al., 2001; Moutin et al., 2012). Our team recently demonstrated an instantaneous disruption of the mGlu5-Homer interaction following membrane depolarization in hippocampal neurons (Moutin et al., 2021), which cannot be explained by the induction of monomeric Homer1a synthesis, a process taking place several minutes later. This depolarization-dependent disruption occurs even if NMDA receptors are blocked (Moutin et al., 2021) and may be attributed to the direct sensitivity of the mGlu5 receptor to membrane potential, as demonstrated in this study. However, testing this hypothesis would require knowledge of and mutations to the voltage sensor of the mGlu5 receptor without affecting the receptor's response to its ligand.

Following the induction of a first plasticity event, the expression of Homer1a blocks the activity of the mGlu5 and NMDA receptors to prevent the induction of subsequent plasticity, allowing cellular signaling required for the expression of the engaged plasticity and the maintenance of the neuron in the functional network in which it has been committed (Moutin et al., 2021). It is worth noting that the direct effect of V_{depol} on mGlu5 receptor functioning described in this study is similar to the effect of Homer1a, which inhibits canonical receptor signaling. The acute effect of depolarization is likely to control the function of the mGlu5 receptor on a shorter time scale. The decreased affinity of the receptor for multimeric Homer, first by membrane depolarization (seconds) and then by CamKII-dependent Homer phosphorylation (minutes, (Guo et al., 2015)), would promote decreased competition and enable the interaction with monomeric Homer1a once this protein is expressed (20-30 minutes, (Moutin et al., 2012)), enabling long-lasting plasticity.

In conclusion, this study has identified mGlu5 receptor as a member of the small yet expanding group of voltage-sensitive GPCRs. The high sensitivity of mGlu5 receptor to changes in membrane potential at synapses suggests that its effects extend beyond canonical signaling and may even impact its cognate NMDA receptor. Optimal functioning of mGlu5 receptor at hyperpolarized potentials could have far-reaching consequences, such as restricting its activation to specific locations by integrating glutamate spill-over and electrical propagation at synapses. Additionally, mGlu5 receptor may exert cell-type-dependent actions, conditioned by the resting potential of cells. Finally, given the crucial role of this receptor in neuronal physiology, it is likely that its voltage sensitivity plays a critical role in pathological conditions associated with variations in intrinsic excitability.

Material and methods

Plasmids

Plasmids were amplified using E.Coli DH5α strain (Life Technologies). DNA was then purified using the NucleoBond® Xtra Plus Midi-Prep kit (Machery-Nagel®). The plasmids used were: pcDNA3.1-rGFP-CAAX (Namkung et al., 2016), pcDNA3.1-p63RhoGEF-RlucII (Avet et al., 2022), pcDNA3.1-Gαq (gift from Jean-Philippe Pin), pRK5-SNAPTag-AT1 (CIS bio international), pRK5-Myc-mGlu5a and pcDNA3.1-Myc-mGlu5a-Venus (Perroy et al., 2008). pCAGGS-TRPC6-ires2-mbtdtomato was obtained by cloning mouse TRPC6 sequence in pCAGGS plasmid (Niwa et al., 1991) upstream the sequences of IRES2 and membrane-anchored tdtomato.

Reagents

(S)-3,5- Dihydroxyphenylglycine (DHPG, HelloBio®); Quisqualate (Tocris); LY341495 (Tocris®); 2-methyl-6-(phenylethynyl)-pyridine hydrochloride (MPEP, HelloBio®); human angiotensin II (HelloBio®); N-Methyl-D-Aspartate (NMDA, Tocris®). 7-(Hydroxyimino)cyclopropa[*b*]chromen-1a-carboxylate ethyl ester (CPCCOEt, Tocris®); Nickel (Merck®); Cadmium (Merck®); 2,3-Dioxo-6-nitro-1,2,3,4-tetrahydrobenzo[f]quinoxaline-7-sulfonamide disodium salt (NBQX, Hellobio®); Tetrodotoxin (TTX) Citrate (Latoxan®), Bicuculline (Hellobio®). Except for dose response curves, all the mGlu5, AT1 and mGlu1 ligands are applied at saturating concentrations.

Cell cultures and transfection

HEK293T cell lines (RRID:CVCL_0063) grown in DMEM GlutaMAX® medium (Gibco™) supplemented with 10% fetal bovine serum and 1% penicillin/streptomycin were maintained at 37°C in a humidity-controlled atmosphere with 5% CO_2. The ST-hmGlu5 HEK293T cell line enables inducible expression of the hmGlu5 receptor containing a SNAP-tagged extracellular VFT domain, as previously described (Ricart-Ortega et al., 2020). Briefly, the release of the constitutive Tet repression of the ST-hmGlu5 gene is induced by doxycycline (Dox), allowing a reproducible and controlled expression, proportional to Dox concentration and incubation time. Cells were maintained in ST-hmGlu5 transgene selection medium in the presence of 100 µg/ml hygromycin B and 15 µg/ml blasticidin. Dox (1µg/ml) was added 6h (Ca^{2+} experiments) or 10 to 24h (TR-FRET measurement) before experiments. Cell lines transduction with the pWPT-EF1a-GcaMP6s-P2A-Scarlet lentivirus (gift from Vincent Compan) enabled stable expression of GcaMP6s fluorescent Ca^{2+} sensor. Plasmids transfection was performed on adherent cells the day after the seeding in antibiotic-free culture medium using Lipofectamine 2000™ (Life Technologies) diluted in OptiMEM GlutaMAX® (Life Technologies) or jetPEI® (Polyplus, only for patch clamp experiments), 24 to 48h before experiments.

Primary cultures of hippocampal neurons were prepared from C57BL/6 mice P0-2 pups as previously described (Moutin et al., 2020). Neurons were seeded onto plastic dishes coated with Poly-L-ornithine (0.03 mg/ml) and laminin (1µg/ml) in Neurobasal, B27, Glutamax, Glutamine, serum and 1% penicillin/streptomycin medium. Neurons were then maintained at 37°C with 5% CO2 and incubated from DIV2 to DIV3 with AraC (1 µM) to inhibit glial cell

proliferation. The medium was then progressively replaced by a serum-free medium (BrainPhys, B27, Glutamax).

Recording Solutions

In all experiments, the extracellular solution contained (in mM): NaCl 140, $CaCl_2$ 2, $MgCl_2$ 0 to 2, KCl 3, HEPES 10, D-glucose 10 (pH = 7.4, 330 mOsm). For neurons, Glycine 0.01, bicuculline 0.01, and tetrodotoxin 0.0003 were added the day of the experiment. For whole-cell voltage clamp recordings, the pipette was filled with an intracellular solution (in mM): CsCl 140, EGTA 5, $CaCl_2$ 0.5, HEPES 10, ATP-Na_2 2 and D-glucose 10 (pH = 7.2, 300 mOsm). Equimolar solutions containing increased KCl concentrations (from 3mM to 100 mM) were obtained by equal decrease of NaCl concentration.

Ca^{2+} measurement

- Cell population: live Ca^{2+} fluctuations were recorded at 37°C on ST-hmGlu5 GcaMP6s-P2A-Scarlet HEK293T cells, or when specified on GcaMP6s-P2A-Scarlet HEK293T cells transfected with pRK-SNAPTag-AT1 (25 ng/well), seeded at 5 x 10^4 cells per well in 96-wells plates with transparent bottom, with the FDSS/µCell plate reader (Hamamatsu®) – Acquisitions of 1Hz; Exc: 480 nm – Em: 540 nm; high-speed digital EM CCD camera. Each independent experiment was performed in triplicate, which average corresponds to n = 1. Data were normalized to the maximum response at V_{rest} in each independent experiment. Basic calculations from the raw data files were performed on Microsoft Excel (Office 2016), statistical analyses and graphics on GraphPad Prism 8.1.

- Single cell imaging: GcaMP6s fluorescence fluctuations were recorded on ST-hmGlu5 GcaMP6s-P2A-Scarlet HEK293T cells, using an Axio Observer 7 KMAT fluorescence microscope (Carl Zeiss), equipped with a Plan-Neofluar 40x/1.30 EC oil objective (M27, ZEISS®), Exc 470/40 nm – Em 525/50 nm filters and ORCA-Quest qCMOS camera (Hamamatsu); all controlled with Metamorph software. Images on HEK cells were acquired at 3Hz and analysed with Fiji using a custom code computing the average fluorescence intensity of the regions of interest. For the frequency analysis, MATLAB was used to automatically detect the oscillations occurrences and compute the instantaneous and global oscillation frequencies. First, baselines were computed as the 10^{th} percentile of the trace using a sliding window of size 400 frames. Signal was then divided by the baseline. Oscillations were detected using the function findpeaks with a minimal peak prominence of 0.01. Instantaneous frequency was computed as the number of oscillations minus one divided by the time between first and last oscillation. Global frequency was computed as the number of oscillations divided by the total duration. Spontaneous Ca^{2+} transients in neurons infected with the pWPT-CAMKIIa-GcaMP6s-P2A-Scarlet lentivirus were acquired at 10 Hz, for series of 2 min and 15 sec. Image stacks were then analyzed as follow: images were filtered with a 5*5 median kernel. Each pixel was divided by its average value over the whole stack. Each pixel was gaussian filtered along the time axis with a sigma of 2 frames. Time derivative was applied to the stack with a step of 6 frames. Images were thresholded with a value of image mean + 6 * image standard deviation. A filter was then applied to keep only voxels with at least 10 thresholded voxels in their 3*3*3 neighborhood, to remove isolated voxels. Thresholded voxels spatially connected were assembled as events. Maximal time projection of those events gave their spatial footprint: the list of pixels in the image. Events with lower than 16 pixels were rejected. Events were classified in different categories based on two criterions: a threshold of 1000 pixels separating

555 big events from small events, a threshold of 0.8 px of propagation distance separating events
556 propagating or not. Propagation distance was measured as the difference of position between
557 the centroid of the pixels thresholded at the beginning and at the end of the onset. Only big
558 events were quantified in **Figure 6**, while both thresholds were applied to focus on "small,
559 non-propagating calcium transients" at synapses in **Figure 8C$_{2\text{-}4}$**. Projection images were
560 obtained by accumulation of the events footprint. Fluorescence time traces were extracted
561 for each event as the average fluorescence over the event pixels and normalized by the
562 fluorescence just before the onset of the event. Area under curve was computed between the
563 onset and 4 seconds later.

564

565 *TR-FRET measurement*

566 TR-FRET measurements were performed as previously described (Scholler et al., 2017). Briefly,
567 ST-hmGlu5 HEK293T seeded at 5 x 10^4 cells per well in 96-wells black bottom plates were
568 incubated for 1h-1h30 with 100nM of SNAP–Lumi4-Tb and/or 60 nM of SNAP–green.
569 Measurements were performed at room temperature using the Pherastar FS (BMG LabTech).
570 Following SNAP–Lumi4-Tb excitation (337 nm), the decays of SNAP–green or SNAP–Lumi4-Tb
571 emission were measured every 10µs at 520 nm and 620 nm respectively. TR-FRET ratios and
572 SNAP–Lumi4-Tb decays were calculated following Scholler et al. recommendation for mGlu
573 receptors with the corresponding time intervals: $\frac{\Sigma\,[50\mu s-100\mu s]}{\Sigma[1200\mu s-1600\mu s]}$ (Scholler et al. 2017). For
574 cells incubated only with SNAP–green, the fluorescence was measured at 520 nm with a 485
575 nm excitation. Each independent experiment was performed in triplicate, which average
576 corresponds to n = 1 and data were normalized to the maximum response at V_{rest} except for
577 LY341495 dose-response curves which were normalized to the maximum response at V_{depol}.

578 Basic calculations from the raw data files were performed on Microsoft Excel (Office 2016),
579 statistical analyses and graphics on GraphPad Prism 8.1.

580

581 *BRET measurement*

582 After coelenterazine H (Coel H, Promega, 2.5 µM) addition, ebBRET measurements in cell
583 population were performed using the LB940Mithras plate reader (Berthold) as previously
584 described (Namkung et al., 2016; Avet et al., 2022), on cells seeded at 5 x 10^4 cells per well in
585 96-wells white bottom plates and transfected with pcDNA3.1-rGFP-CAAX (33,3 ng/well),
586 pcDNA3.1-p63RhoGEF-RlucII (5,1 ng/well), pcDNA3.1-Gαq (6,75 ng/well) combined with the
587 pRK5-Myc-mGlu5a (14,7 ng/well) or pRK-SNAPtag-AT1 (14,8 ng/well). BRET, or the 535
588 nm/485 nm ratio, was assessed by calculating the ratio of the light emitted by the acceptor
589 (510–550 nm band-pass filter, Em535) to the light emitted by the donor (460–500 nm band-
590 pass filter, Em480).

591 Single cell BRET imaging was previously described (Goyet et al., 2016). Acquisitions were
592 performed on cells seeded in 35mm diameter glass dishes (MatTek® for microscopy) coated
593 with poly-ornithine (0.03 mg/ml, for 30min), after Coel H (5 µM) addition, using the Axio
594 Observer 7 KMAT fluorescence microscope (Carl Zeiss), equipped with a Neofluar 40X/1.3
595 planar EC oil objective (M27, ZEISS) and an ORCA-Quest qCMOS camera (Hamamatsu),
596 controlled by Metamorph software. The emission of RlucII (10s exposure, FF01-450nm/70-25
597 Brightline filter, Semrock) and rGFP (20s exposure, HQ535nm/50M filter, Chroma Technology
598 Corp) were measured successively. Images were analyzed using the BRET Analyzer macro on
599 Fiji (Chastagnier et al., 2018). Overall, this analysis uses an open-source toolkit for Fiji
600 (https://github.com/ychastagnier/BRET-Analyzer) performing four key steps in the analysis:

(1) background subtraction from the image, (2) image alignment over time, (3) composite thresholding of the image, and (4) pixel-by-pixel division of the image and distribution of the BRET ratio intensity on a pseudo-color scale. The BRET ratio corresponds to the acceptor/donor emission ratio (535/450).

Electrophysiology

HEK293T cells, seeded in 35 mm diameter plastic dishes at low confluency ($1x10^4$ cells) and transfected with pcDNA3.1-Myc-mGlu5-Venus (0.25 µg) and pCAGGS-TRPC6-ires2-mbtdtomato (0.5 µg) plasmids, were targeted by fluorescence microscopy. Measurements were performed in the whole cell configuration, in voltage or current clamp mode, with pipettes of 2-4 MΩ resistance when filled with the appropriate intracellular medium.

At 10 to 12 days in vitro, hippocampal neurons were used for endogenous NMDA current measurements. Patch clamp recordings were performed in the whole-cell configuration with pipettes of 3-5 MΩ resistance when filled with the appropriate intracellular medium. NMDA stimulations were separated by 2 min to avoid receptor desensitization. All recordings were performed at room temperature for less than 1 h per dish. Drugs were applied using a gravity perfusion system allowing complete exchange of the cellular environment in less than 30ms. Currents were recorded using an Axopatch 200B amplifier (Axon Instruments), with noise removal at 50-60 Hz (Hum Bug Noise, Quest Scientific) and digitized at 3 kHz before being stored in Clampex software (version 8.1). The data were then analyzed using the Clampfit 11.2 software from Axon instruments (Molecular Devices).

Data and analysis

The statistical tests are indicated in each of the figure legends. Statistical analysis was undertaken only for studies where each group size was at least n=5. Studies were designed to generate groups of equal size, using randomisation and blinded analysis. Group size is the number of independent values, and statistical analysis was done using these independent values. p= 0.05 was the level of probability to constitute the threshold for statistical significance for determining whether groups differ. Outliers were included in data analysis and presentation. The manuscript complies with BJP's recommendations and requirements on experimental design and analysis (Curtis MJ, Alexander S, Cirino G, Docherty JR, George CH, Giembycz MA, Hoyer D, Insel PA, Izzo AA, Ji Y, MacEwan DA, Sobey CG, Stanford SC, Teixeira MM, Wonnacott S, Ahluwalia A. Experimental design and analysis and their reporting II: updated and simplified guidance for authors and peer reviewers. Br J Pharmacology 175 987–993, 2018).

Nomenclature of Targets and Ligands

Key protein targets and ligands in this article are hyperlinked to corresponding entries in http://www.guidetopharmacology.org, and are permanently archived in the Concise Guide to PHARMACOLOGY 2021/22(151-157).

Acknowledgments

The authors thank the iExplore animal facility (IGF, Montpellier) and the Arpege platform (IGF, Montpellier) for the use of plate reader fluorimeter for cell-population BRET and FRET assay. The authors thank Philippe Marin, Jean-Philippe Pin, Laurent Prézeau, Charlotte Avet and Michel Bouvier for providing biosensors and helpful discussions. We are grateful to Charlotte Sarre for the mGlu5 receptor graphic design. This work was supported by the Agence Nationale de la Recherche (JP, ANR-22-CE16-0013 LEARN), the Fondation pour la recherche médicale (FRM, JP, grant agreement No. EQU202303016311) and the European Research Council (ERC) under the European Union's Horizon 2020 research and innovation programme (JP, grant agreement No. 646788 VERTICAL CITY).

Author contributions

MB and JP conceived research and wrote the manuscript; MB carried out the majority of the experiments, conception, design of the protocols, analysis of the results and production of the figures. CC carried out G protein sensor experiments, including protocol design, experiments and analyses. NB performed theoretical and manual supervision of the molecular biology experiments (electrophoresis, plasmid digestion, transfection) and data interpretation. YC provided general assistance with the acquisition and analysis of results in microscopy, he also developed optimised programmes to facilitate and automate signal analysis. JFI helped to design and perform experiments to detect mGlu5 receptor conformation. EM supervised and implemented neuronal cultures with NB and the development of population BRET protocols. LT cloned the pCAGGS-TRPC6-ires2-mbtdtomato plasmid. JC took an active part in the implementation of the experimental protocol and together with LT provided advices for patch clamp recordings on HEK and analysis of results. JP carried out BRET and calcium microscopy

experiments in neurons, and was involved in the analysis of results and theoretical supervision at all levels. JP conceived and supervised the full project. All authors contribute to the preparation of the manuscript and approved it.

Competing Interests Statement

None - The authors declare no competing interests.

Declaration of transparency and scientific rigour

This Declaration acknowledges that this paper adheres to the principles for transparent reporting and scientific rigour of preclinical research as stated in the BJP guidelines for Design and Analysis, and as recommended by funding agencies, publishers and other organisations engaged with supporting research.

References

Acker, C. D., Hoyos, E., and Loew, L. M. (2016). EPSPs measured in proximal dendritic spines of cortical pyramidal neurons. *eNeuro* 3. doi: 10.1523/ENEURO.0050-15.2016.

Ango, F., Prézeau, L., Muller, T., Tu, J. C., Xiao, B., Worley, P. F., et al. (2001). Agonist-independent activation of metabotropic glutamate receptors by the intracellular protein Homer. *Nature* 411. doi: 10.1038/35082096.

Aniksztejn, L., Otani, S., and Ben-Ari, Y. (1992). Quisqualate Metabotropic Receptors Modulate NMDA Currents and Facilitate Induction of Long-Term Potentiation Through Protein Kinase C. *European Journal of Neuroscience* 4. doi: 10.1111/j.1460-9568.1992.tb00900.x.

Avet, C., Mancini, A., Breton, B., Gouill, C. Le, Hauser, A. S., Normand, C., et al. (2022). Effector membrane translocation biosensors reveal G protein and Parrestin coupling profiles of 100 therapeutically relevant GPCRs. *Elife* 11. doi: 10.7554/eLife.74101.

Barchad-Avitzur, O., Priest, M. F., Dekel, N., Bezanilla, F., Parnas, H., and Ben-Chaim, Y. (2016). A Novel Voltage Sensor in the Orthosteric Binding Site of the M2 Muscarinic Receptor. *Biophys J* 111. doi: 10.1016/j.bpj.2016.08.035.

Ben-Chaim, Y., Chanda, B., Dascal, N., Bezanilla, F., Parnas, I., and Parnas, H. (2006). Movement of "gating charge" is coupled to ligand binding in a G-protein-coupled receptor. *Nature* 444. doi: 10.1038/nature05259.

Ben-Chaim, Y., Tour, O., Dascal, N., Parnas, I., and Parnas, H. (2003). The M2 muscarinic G-protein-coupled receptor is voltage-sensitive. *Journal of Biological Chemistry* 278. doi: 10.1074/jbc.M301146200.

Benquet, P., Gee, C. E., and Gerber, U. (2002). Two distinct signaling pathways upregulate NMDA receptor responses via two distinct metabotropic glutamate receptor subtypes. *Journal of Neuroscience* 22. doi: 10.1523/jneurosci.22-22-09679.2002.

Birk, A., Rinne, A., and Bünemann, M. (2015). Membrane potential controls the efficacy of catecholamineinduced β1-Adrenoceptor activity. *Journal of Biological Chemistry* 290, 27311–27320. doi: 10.1074/jbc.M115.665000.

Bockaert, J., Perroy, J., and Ango, F. (2021). The complex formed by group i metabotropic glutamate receptor (MGLUR) and homer1a plays a central role in metaplasticity and homeostatic synaptic scaling. *Journal of Neuroscience* 41. doi: 10.1523/JNEUROSCI.0026-21.2021.

Bradley, S. J., Langmead, C. J., Watson, J. M., and Challiss, R. A. J. (2011). Quantitative analysis reveals multiple mechanisms of allosteric modulation of the mGlu5 receptor in rat astroglia. *Mol Pharmacol* 79. doi: 10.1124/mol.110.068882.

Bradley, S. J., Watson, J. M., and Challiss, R. A. J. (2009). Effects of positive allosteric modulators on single-cell oscillatory Ca2+ signaling initiated by the type 5 metabotropic glutamate receptor. *Mol Pharmacol* 76. doi: 10.1124/mol.109.059170.

Chastagnier, Y., Moutin, E., Hemonnot, A. L., and Perroy, J. (2018). Image processing for bioluminescence resonance energy transfer measurement-BRET-Analyzer. *Front Comput Neurosci* 11. doi: 10.3389/fncom.2017.00118.

719 Chiu, D. N., and Carter, B. C. (2022). Synaptic NMDA receptor activity at resting membrane potentials.
720 *Front Cell Neurosci* 16. doi: 10.3389/fncel.2022.916626.

721 Cornejo, V. H., Ofer, N., and Yuste, R. (2022). Voltage compartmentalization in dendritic spines in
722 vivo. *Science (1979)* 375. doi: 10.1126/science.abg0501.

723 David, D., Bentulila, Z., Tauber, M., and Ben-Chaim, Y. (2022). G Protein-Coupled Receptors Regulated
724 by Membrane Potential. *Int J Mol Sci* 23. doi: 10.3390/ijms232213988.

725 Diering, G. H., Nirujogi, R. S., Roth, R. H., Worley, P. F., Pandey, A., and Huganir, R. L. (2017). Homer1a
726 drives homeostatic scaling-down of excitatory synapses during sleep. *Science (1979)* 355. doi:
727 10.1126/science.aai8355.

728 Ding, F., O'donnell, J., Xu, Q., Kang, N., Goldman, N., and Nedergaard, M. (2016). Changes in the
729 composition of brain interstitial ions control the sleep-wake cycle. *Science (1979)* 352. doi:
730 10.1126/science.aad4821.

731 Doumazane, E., Scholler, P., Fabre, L., Zwier, J. M., Trinquet, E., Pin, J. P., et al. (2013). Illuminating
732 the activation mechanisms and allosteric properties of metabotropic glutamate receptors. *Proc*
733 *Natl Acad Sci U S A* 110, E1416-25. doi: 10.1073/pnas.1215615110.

734 Dryer, S. E., and Kim, E. Y. (2018). Permeation and rectification in canonical transient receptor
735 potential-6 (TRPC6) channels. *Front Physiol* 9. doi: 10.3389/fphys.2018.01055.

736 Francesconi, W., Cammalleri, M., and Sanna, P. P. (2004). The metabotropic glutamate receptor 5 is
737 necessary for late-phase long-term potentiation in the hippocampal CA1 region. *Brain Res* 1022.
738 doi: 10.1016/j.brainres.2004.06.060.

739 García-Sáinz, J. A., Martínez-Alfaro, M., Romero-Avila, M. T., and González-Espinosa, C. (1997).
740 Characterization of the AT1 angiotensin II receptor expressed in guinea pig liver. *Journal of*
741 *Endocrinology* 154. doi: 10.1677/joe.0.1540133.

742 Gómez-Santacana, X., Pittolo, S., Rovira, X., Lopez, M., Zussy, C., Dalton, J. A. R., et al. (2017).
743 Illuminating Phenylazopyridines to Photoswitch Metabotropic Glutamate Receptors: From the
744 Flask to the Animals. *ACS Cent Sci* 3. doi: 10.1021/acscentsci.6b00353.

745 Goyet, E., Bouquier, N., Ollendorff, V., and Perroy, J. (2016). Fast and high resolution single-cell BRET
746 imaging. *Sci Rep* 6, 28231. doi: 10.1038/srep28231.

747 Guo, W., Ceolin, L., Collins, K. A., Perroy, J., and Huber, K. M. (2015). Elevated CaMKIIalpha and
748 Hyperphosphorylation of Homer Mediate Circuit Dysfunction in a Fragile X Syndrome Mouse
749 Model. *Cell Rep* 13, 2297–2311. doi: 10.1016/j.celrep.2015.11.013.

750 Heidinger, V., Manzerra, P., Wang, X. Q., Strasser, U., Yu, S. P., Choi, D. W., et al. (2002).
751 Metabotropic glutamate receptor 1-induced upregulation of NMDA receptor current:
752 Mediation through the Pyk2/Src-family kinase pathway in cortical neurons. *Journal of*
753 *Neuroscience* 22. doi: 10.1523/jneurosci.22-13-05452.2002.

754 Hof, T., Chaigne, S., Récalde, A., Sallé, L., Brette, F., and Guinamard, R. (2019). Transient receptor
755 potential channels in cardiac health and disease. *Nat Rev Cardiol* 16. doi: 10.1038/s41569-018-
756 0145-2.

Holz, A., Mülsch, F., Schwarz, M. K., Hollmann, M., Döbrössy, M. D., Coenen, V. A., et al. (2019). Enhanced mGlu5 Signaling in Excitatory Neurons Promotes Rapid Antidepressant Effects via AMPA Receptor Activation. *Neuron* 104. doi: 10.1016/j.neuron.2019.07.011.

Hoppe, A., Marti-Solano, M., Drabek, M., Bünemann, M., Kolb, P., and Rinne, A. (2018). The allosteric site regulates the voltage sensitivity of muscarinic receptors. *Cell Signal* 42. doi: 10.1016/j.cellsig.2017.10.011.

Hu, J. H., Park, J. M., Park, S., Xiao, B., Dehoff, M. H., Kim, S., et al. (2010). Homeostatic Scaling Requires Group I mGluR Activation Mediated by Homer1a. *Neuron* 68. doi: 10.1016/j.neuron.2010.11.008.

Inuzuka, T., Fujioka, Y., Tsuda, M., Fujioka, M., Satoh, A. O., Horiuchi, K., et al. (2016). Attenuation of ligand-induced activation of angiotensin II type 1 receptor signaling by the type 2 receptor via protein kinase C. *Sci Rep* 6. doi: 10.1038/srep21613.

Itsuki, K., Imai, Y., Hase, H., Okamura, Y., Inoue, R., and Mori, M. X. (2014). PLC-mediated PI(4,5)P2 hydrolysis regulates activation and inactivation of TRPC6/7 channels. *Journal of General Physiology* 143. doi: 10.1085/jgp.201311033.

Jayant, K., Hirtz, J. J., Plante, I. J. La, Tsai, D. M., De Boer, W. D. A. M., Semonche, A., et al. (2017). Targeted intracellular voltage recordings from dendritic spines using quantum-dot-coated nanopipettes. *Nat Nanotechnol* 12. doi: 10.1038/nnano.2016.268.

Kupchik, Y. M., Barchad-Avitzur, O., Wess, J., Ben-Chaim, Y., Parnas, I., and Parnas, H. (2011). A novel fast mechanism for GPCR-mediated signal transduction - Control of neurotransmitter release. *Journal of Cell Biology* 192. doi: 10.1083/jcb.201007053.

Kurz, M., Krett, A. L., and Bünemann, M. (2020). Voltage dependence of prostanoid receptors. *Mol Pharmacol* 97. doi: 10.1124/mol.119.118372.

Kwag, J., and Paulsen, O. (2012). Gating of NMDA receptor-mediated hippocampal spike timing-dependent potentiation by mGluR5. *Neuropharmacology* 63. doi: 10.1016/j.neuropharm.2012.05.021.

Lagerström, M. C., and Schiöth, H. B. (2008). Erratum: Structural diversity of G protein-coupled receptors and significance for drug discovery. *Nat Rev Drug Discov* 7. doi: 10.1038/nrd2592.

Lepannetier, S., Gualdani, R., Tempesta, S., Schakman, O., Seghers, F., Kreis, A., et al. (2018). Activation of TRPC1 Channel by Metabotropic Glutamate Receptor mGluR5 Modulates Synaptic Plasticity and Spatial Working Memory. *Front Cell Neurosci* 12. doi: 10.3389/fncel.2018.00318.

Lin, M. Z., and Schnitzer, M. J. (2016). Genetically encoded indicators of neuronal activity. *Nat Neurosci* 19. doi: 10.1038/nn.4359.

López-Serrano, A. L., De Jesús-Pérez, J. J., Zamora-Cárdenas, R., Ferrer, T., Rodríguez-Menchaca, A. A., Tristani-Firouzi, M., et al. (2020). Voltage-induced structural modifications on M2 muscarinic receptor and their functional implications when interacting with the superagonist iperoxo. *Biochem Pharmacol* 177. doi: 10.1016/j.bcp.2020.113961.

Lutzu, S., and Castillo, P. E. (2021). Modulation of NMDA Receptors by G-protein-coupled receptors: Role in Synaptic Transmission, Plasticity and Beyond. *Neuroscience* 456. doi: 10.1016/j.neuroscience.2020.02.019.

Mannaioni, G., Marino, M. J., Valenti, O., Traynelis, S. F., and Conn, P. J. (2001). Metabotropic glutamate receptors 1 and 5 differentially regulate CA1 pyramidal cell function. *Journal of Neuroscience* 21. doi: 10.1523/jneurosci.21-16-05925.2001.

Martinez-Pinna, J., Gurung, I. S., Vial, C., Leon, C., Gachet, C., Evans, R. J., et al. (2005). Direct voltage control of signaling via P2Y1 and other Gαq-coupled receptors. *Journal of Biological Chemistry* 280. doi: 10.1074/jbc.M407783200.

Mølck, C., Harpsøe, K., Gloriam, D. E., Clausen, R. P., Madsen, U., Pedersen, L., et al. (2012). Pharmacological characterization and modeling of the binding sites of novel 1,3-Bis(pyridinylethynyl)benzenes as metabotropic glutamate receptor 5-selective negative allosteric modulators. *Mol Pharmacol* 82. doi: 10.1124/mol.112.078808.

Moutin, E., Hemonnot, A. L., Seube, V., Linck, N., Rassendren, F., Perroy, J., et al. (2020). Procedures for Culturing and Genetically Manipulating Murine Hippocampal Postnatal Neurons. *Front Synaptic Neurosci* 12. doi: 10.3389/fnsyn.2020.00019.

Moutin, E., Raynaud, F., Roger, J., Pellegrino, E., Homburger, V., Bertaso, F., et al. (2012). Dynamic remodeling of scaffold interactions in dendritic spines controls synaptic excitability. *Journal of Cell Biology* 198, 251–263. doi: 10.1083/jcb.201110101.

Moutin, E., Sakkaki, S., Compan, V., Bouquier, N., Giona, F., Areias, J., et al. (2021). Restoring glutamate receptosome dynamics at synapses rescues autism-like deficits in Shank3-deficient mice. *Mol Psychiatry*. doi: 10.1038/s41380-021-01230-x.

Nagy, G. A., Botond, G., Borhegyi, Z., Plummer, N. W., Freund, T. F., and Hájos, N. (2013). DAG-sensitive and Ca2+ permeable TRPC6 channels are expressed in dentate granule cells and interneurons in the hippocampal formation. *Hippocampus* 23. doi: 10.1002/hipo.22081.

Nakahara, K., Okada, M., and Nakanishi, S. (1997). The metabotropic glutamate receptor mGluR5 induces calcium oscillations in cultured astrocytes via protein kinase C phosphorylation. *J Neurochem* 69. doi: 10.1046/j.1471-4159.1997.69041467.x.

Namkung, Y., Le Gouill, C., Lukashova, V., Kobayashi, H., Hogue, M., Khoury, E., et al. (2016). Monitoring G protein-coupled receptor and β-arrestin trafficking in live cells using enhanced bystander BRET. *Nat Commun* 7. doi: 10.1038/ncomms12178.

Nash, M. S., Schell, M. J., Atkinson, P. J., Johnston, N. R., Nahorski, S. R., and John Challiss, R. A. (2002). Determinants of metabotropic glutamate receptor-5-mediated Ca 2+ and inositol 1,4,5-trisphosphate oscillation frequency: Receptor density versus agonist concentration. *Journal of Biological Chemistry* 277. doi: 10.1074/jbc.M205622200.

Nasrallah, C., Cannone, G., Briot, J., Rottier, K., Berizzi, A. E., Huang, C. Y., et al. (2021). Agonists and allosteric modulators promote signaling from different metabotropic glutamate receptor 5 conformations. *Cell Rep* 36. doi: 10.1016/j.celrep.2021.109648.

Navarro-Polanco, R. A., Aréchiga-Figueroa, I. A., Salazar-Fajardo, P. D., Benavides-Haro, D. E., Rodríguez-Elías, J. C., Sachse, F. B., et al. (2013). Voltage sensitivity of M2 muscarinic receptors underlies the delayed rectifier-like activation of ACh-gated K+ current by choline in feline atrial myocytes. *Journal of Physiology* 591. doi: 10.1113/jphysiol.2013.255166.

Navarro-Polanco, R. A., Galindo, E. G. M., Ferrer-Villada, T., Arias, M., Rigby, J. R., Sánchez-Chapula, J. A., et al. (2011). Conformational changes in the M2 muscarinic receptor induced by membrane voltage and agonist binding. *Journal of Physiology* 589. doi: 10.1113/jphysiol.2010.204107.

Neyman, S., and Manahan-Vaughan, D. (2008). Metabotropic glutamate receptor 1 (mGluR1) and 5 (mGluR5) regulate late phases of LTP and LTD in the hippocampal CA1 region in vitro. *European Journal of Neuroscience* 27. doi: 10.1111/j.1460-9568.2008.06109.x.

Niswender, C. M., and Conn, P. J. (2010). Metabotropic glutamate receptors: Physiology, pharmacology, and disease. *Annu Rev Pharmacol Toxicol* 50. doi: 10.1146/annurev.pharmtox.011008.145533.

Niwa, H., Yamamura, K., and Miyazaki, J. (1991). Efficient selection for high-expression transfectants with a novel eukaryotic vector. *Gene* 108.

Ohana, L., Barchad, O., Parnas, I., and Parnas, H. (2006). The metabotropic glutamate G-protein-coupled receptors mGluR3 and mGluR1a are voltage-sensitive. *Journal of Biological Chemistry* 281. doi: 10.1074/jbc.M513447200.

O'Malley, K. L., Jong, Y. J. I., Gonchar, Y., Burkhalter, A., and Romano, C. (2003). Activation of metabotropic glutamate receptor mGlu5 on nuclear membranes mediates intranuclear Ca2+ changes in heterologous cell types and neurons. *Journal of Biological Chemistry* 278. doi: 10.1074/jbc.M300792200.

O'neill, N., McLaughlin, C., Komiyama, N., and Sylantyev, S. (2018). Biphasic modulation of NMDA receptor function by metabotropic glutamate receptors. *Journal of Neuroscience* 38. doi: 10.1523/JNEUROSCI.1000-18.2018.

Perroy, J., Raynaud, F., Homburger, V., Rousset, M. C., Telley, L., Bockaert, J., et al. (2008). Direct interaction enables cross-talk between ionotropic and group I metabotropic glutamate receptors. *Journal of Biological Chemistry*. doi: 10.1074/jbc.M705661200.

Pisani, A., Calabresi, P., Centonze, D., and Bernardi, G. (1997). Enhancement of NMDA responses by group I metabotropic glutamate receptor activation in striatal neurones. *Br J Pharmacol* 120. doi: 10.1038/sj.bjp.0700999.

Rae, M. G., Martin, D. J., Collingridge, G. L., and Irving, A. J. (2000). Role of Ca2+ stores in metabotropic L-glutamate receptor-mediated supralinear Ca2+ signaling in rat hippocampal neurons. *Journal of Neuroscience* 20. doi: 10.1523/jneurosci.20-23-08628.2000.

Reiner, A., and Levitz, J. (2018). Glutamatergic Signaling in the Central Nervous System: Ionotropic and Metabotropic Receptors in Concert. *Neuron* 98. doi: 10.1016/j.neuron.2018.05.018.

Ricart-Ortega, M., Berizzi, A. E., Catena, J., Malhaire, F., Muñoz, L., Serra, C., et al. (2020). Development and validation of a mass spectrometry binding assay for mGlu5 receptor. *Anal Bioanal Chem* 412. doi: 10.1007/s00216-020-02772-9.

Rinne, A., Mobarec, J. C., Mahaut-Smith, M., Kolb, P., and Bünemann, M. (2015). The mode of agonist binding to a G protein-coupled receptor switches the effect that voltage changes have on signaling. *Sci Signal* 8. doi: 10.1126/scisignal.aac7419.

Rössig, L., Zólyomi, A., Catt, K. J., and Balla, T. (1996). Regulation of angiotensin II-stimulated Ca2+ oscillations by Ca2+ influx mechanisms in adrenal glomerulosa cells. *Journal of Biological Chemistry* 271. doi: 10.1074/jbc.271.36.22063.

Rozenfeld, E., Tauber, M., Ben-Chaim, Y., and Parnas, M. (2021). GPCR voltage dependence controls neuronal plasticity and behavior. *Nat Commun* 12. doi: 10.1038/s41467-021-27593-x.

Ruland, J. G., Kirchhofer, S. B., Klindert, S., Bailey, C. P., and Bünemann, M. (2020). Voltage modulates the effect of μ-receptor activation in a ligand-dependent manner. *Br J Pharmacol* 177. doi: 10.1111/bph.15070.

Sahlholm, K., Nilsson, J., Marcellino, D., Fuxe, K., and Århem, P. (2008). Voltage-dependence of the human dopamine D2 receptor. *Synapse* 62. doi: 10.1002/syn.20509.

Scheefhals, N., and MacGillavry, H. D. (2018). Functional organization of postsynaptic glutamate receptors. *Molecular and Cellular Neuroscience* 91. doi: 10.1016/j.mcn.2018.05.002.

Scholler, P., Moreno-Delgado, D., Lecat-Guillet, N., Doumazane, E., Monnier, C., Charrier-Savournin, F., et al. (2017). HTS-compatible FRET-based conformational sensors clarify membrane receptor activation. *Nat Chem Biol* 13. doi: 10.1038/nchembio.2286.

SEEBURG, P. H., BURNASHEV, N., KÖHR, G., KUNER, T., SPRENGEL, R., and MONYER, H. (1995). "The NMDA Receptor Channel: Molecular Design of a Coincidence Detector," in *Proceedings of the 1993 Laurentian Hormone Conference* doi: 10.1016/b978-0-12-571150-0.50006-8.

Sobczyk, A., Scheuss, V., and Svoboda, K. (2005). NMDA receptor subunit-dependent [Ca2+] signaling in individual hippocampal dendritic spines. *Journal of Neuroscience* 25. doi: 10.1523/JNEUROSCI.1221-05.2005.

Wang, Q., Wang, D., Shibata, S., Ji, T., Zhang, L., Zhang, R., et al. (2019). Group I metabotropic glutamate receptor activation induces TRPC6-dependent calcium influx and RhoA activation in cultured human kidney podocytes. *Biochem Biophys Res Commun* 511. doi: 10.1016/j.bbrc.2019.02.062.

Zhang, Q., Liu, B., Li, Y., Yin, L., Younus, M., Jiang, X., et al. (2020). Regulating quantal size of neurotransmitter release through a GPCR voltage sensor. *Proc Natl Acad Sci U S A* 117. doi: 10.1073/pnas.2005274117.

Figure titles and legends

Graphical Abstract

mGlu5 receptor function is optimal at resting cell potential. Membrane depolarization stabilizes an inactive-like conformation of mGlu5 receptor and decreases agonist-induced G_q

protein activation, Ca^{2+} release from intracellular stores and gating of NMDA and TRPC6 channels.

Figure 1. Voltage regulates mGlu5 agonist-induced Ca^{2+} release. HEK cells stably expressing GCaMP6s also transiently expressed mGlu5 (B-F) or AT1 (G) receptors. **A)** Scheme of GCaMP6s fluorescent Ca^{2+} sensor - adapted from (Lin and Schnitzer, 2016). GCaMP6s is composed of a circularly permuted GFP, a calmodulin (CaM) and a peptide from smooth-muscle myosin light-chain kinase (RS20). **B)** DHPG (100µM)-induced fluorescence fluctuation in cells expressing (black and blue) or not (grey) mGlu5 receptor, in absence (grey and black) or presence (blue) of the mGlu5 NAM, MPEP (10µM); Representative illustration. **C)** Peak of fluorescence fluctuation induced by quisqualate (10µM) in isotonic extracellular solutions containing increasing KCl concentrations ([KCl] in mM), normalized to fluorescence fluctuations recorded with the 3mM [KCl] solution. Data are mean ± SEM of n = 6 triplicates from independent experiments. Statistics: Kruskal-Wallis test, **D)** Membrane potential measured in the current clamp whole-cell configuration with extracellular solutions containing either 3mM (black) or 100mM (red) KCl. Data are mean ± SEM of n = 10 cells from 5 independent experiments. Statistics: Friedman test **E)** Dose-response curves of DHPG-induced fluorescence fluctuation with KCl 3mM (black, V_{rest}) and 100mM (red, V_{depol}), normalized to V_{rest} peak of each experiment. Data are mean ± SEM of n = 3 independent experiments. **F** and **G)** Quisqualate (10µM, F) or Angiotensine II (1µM, G) -induced fluorescence fluctuation in KCl 3mM (V_{rest}) and 100mM (V_{depol}) solutions. Left, representative illustration; Right, mean ± SEM of n = 7 to 14 triplicates from independent experiments; Statistics: one sample Wilcoxon test.

Figure 2. Voltage regulates mGlu5 agonist-induced Ca^{2+} oscillations. A) Representative field of GCaMP6s expressing cells in epifluorescence microscopy - Scale = 10 µm. **B)** Quisqualate (10µM)-induced fluorescence fluctuation at V_{rest} (left, black) and V_{depol} (middle, red), for individual field of view (thin) and average (thick) aligned to the peak of response, and quantification of the mean ± SEM of n = 14 to 21 independent experiments (right, Statistics: Mann-Whitney test) **C)** Fluorescence fluctuation recorded in representative oscillating, single spike and silent cells at V_{rest} and V_{depol} in response to quisqualate (10µM) with proportion of cells in each category displayed in a circular diagram, n = 403 cells for V_{rest} and 324 cells for V_{depol} **D)** Percentage of oscillating cells (> 2 oscillations) at V_{rest} and V_{depol}. n = 324 to 403 cells from 14 to 18 independent experiments. Statistics: N-1 χ^2 test, p = 0.0001. **E)** Violin plots with mean indicated by a dotted line of global frequency of fluorescence oscillations induced by quisqualate (10µM) application at V_{rest} and V_{depol} (n = 280 to 408 cells). Statistics: unpaired t-test. **F)** Representative illustrations (left) and violin plots with mean indicated by a dotted line (right) of fluorescence oscillations frequency induced by V_{rest} or V_{depol} imposed after quisqualate (10µM) application (n = 21 to 35 cells - Statistics: unpaired t-test)

Figure 3. Voltage tunes mGlu5 receptor activation probability. **A)** Scheme of the TR-FRET sensor of mGlu5 conformation (Doumazane et al., 2013) with SNAP-Lumi4-Tb (purple) and SNAP-fluoroscein (green) linked on SNAP-tag-mGlu5 VFT domains. The FRET signal is inversely proportional to the number of receptors in an active-like conformation. **B)** TR-FRET intensity at V_{rest} with and without quisqualate 10µM (left) and quisqualate (10µM) effect at V_{rest} and V_{depol} (right). Data are mean ± SEM of n = 10 independent experiments. Statistics: Wilcoxon

test. **C)** Dose-response curve of LY341495 mGlu antagonist applied at V_{rest} or V_{depol}. Data are mean ± SEM of n = 4 independent experiments normalized to the maximum TR-FRET of V_{depol}.

Figure 4. Voltage modulates mGlu5-mediated Gq activation. A) Scheme of EMTA ebBRET sensor of Gq activation (Avet et al., 2022). When Gq is activated by mGlu5, p63-RhoGEF-RlucII is recruited to the membrane where it interacts with rGFP-CAAX. **B** and **C)** Representative illustrations (B) and mean ± SEM (C) of BRET signals measured before (CT) and after (DHPG, 100µM) stimulation at V_{rest} or V_{depol}. N= 86 to 97 cells from more than 5 independent experiments; statistics: Paired t-test. **D)** Violin plots with mean indicated by a dotted line of single cell BRET measurement of DHPG net effect; statistics: Unpaired t-test.

Figure 5. Voltage controls mGlu5 gating of TRPC6 channels. A and **B) -** Whole-cell patch clamp current induced by DHPG (100µM) on HEK293T cells expressing mGlu5-Venus alone (A) or with TRPC6-tomato (B). **C)** mGlu5-Venus/TRPC6-tomato co-transfected cells were held at -80mV (black) or -20mV (red) during DHPG (100µM) application. Current-voltage relationship was then recorded at the maximum response induced by DHPG (100µM) for potentials ranging from -80mV to +60mV in 100ms (bottom). Inset: Mean ± SEM current density at -80mV. Data are mean ± SEM of n = 9 cells per condition from 5 independent experiments, Statistics: Mann-Whitney test.

Figure 6. Voltage regulates mGlu5 agonist-induced Ca^{2+} oscillations in hippocampal neurons. Projection of spontaneous calcium transients, in presence of Nickel, Cadmium, NBQX, AP5 and

CPCCOEt, recorded at V_{rest} (black) and V_{depol} (red) during sequential acquisitions (1 min and 30 sec) before (faded colors) and after (dark colors) DHPG application. **A)** representative illustration, **B)** measure of fluorescence fluctuation in representative neurons, stimulated (DHPG) or not (CT) just before recording **C)** violin plots with mean indicated by a dotted line of the number of events (n = 5 to 7 independent experiments - Statistics: Mann-Whitney test)

Figure 7. Voltage regulates mGlu5 gating of NMDA receptor in hippocampal neurons. A) Representative current and mean density induced by DHPG (50µM, left) or NMDA (30µM, right) at -80mV. **B - D)** Representative currents (B), mean current density and $I_{NMDA+DHPG}/I_{NMDA}$ current ratio (C), and percentage of DHPG-induced NMDA current potentiation (D) measured in presence of NMDA (30µM) alone or co-applied with DHPG (50µM) at -80mV (black) and -40mV (red) holding potential. Measures of I_{NMDA} (blue) and $I_{NMDA+DHPG}$ (black) used for quantification in C and D are indicated by arrows in B. In D, paired measurement of $I_{NMDA + DHPG}$ / I_{NMDA} were performed subsequently at -80mV or -40mV, in a random order, on the same neuron. C and D data are mean ± SEM of n = 10 to 15 neurons from at least 5 independent experiments; Statistics: Wilcoxon matched-pairs signed rank test.

Figure 8. DHPG-induced potentiation of NMDA currents at resting potential, in physiological concentration of Mg^{2+}.

A) Left - Representative NMDA (100µM)-induced current, without (NMDA) or with (Mg^{2+}) extracellular Mg^{2+} (0.7 mM), co-applied with DHPG (50 µM). Right – Mean ± SEM current density recorded in 0.7 mM Mg^{2+}, from n = 21 neurons in 5 independent experiments. Wilcoxon matched-pairs signed rank test. **B)** Current density-voltage relationship (-80 -> +60

mV within 100ms every 5s) performed as illustrated in (a) during NMDA application (at the plateau response) without (blue) or with 0.7 mM Mg^{2+} (black) co-applied with DHPG (red). Mean from n = 8-10 neurons per condition. **C)** Projection of spontaneous calcium transients, recorded during 2 min and 15 sec, in Mg^{2+} (0.7mM) at resting potential of neurons in a representative field of view. **C_1**: all events for the entire field of view. **C_{2-4}**: small non-propagating calcium transients from the white square in C_1, recorded during three consecutive acquisitions, in control conditions C_2, and following application of DHPG (50 µM, C_3) and AP5 (50 µM, C_4). **D)** Number of calcium transients recorded in the whole field of view before (CT) and after sequential application of DHPG and AP5. **E)** Mean area under curve (AUC) of calcium transients. Each bar of the histogram is the Mean ± SEM of all AUC traces recorded in the whole field of view before and after DHPG application for 2 min and 15 seconds in both conditions. Statistics: Unpaired t test. **F)** GCaMP6s fluorescence fluctuation during small non-propagating calcium transients; Mean ± SEM of 91 and 94 traces, before (black) and after (red) DHPG application, measured on 10, identical, AP5-sensitive ROI;

Figure 1

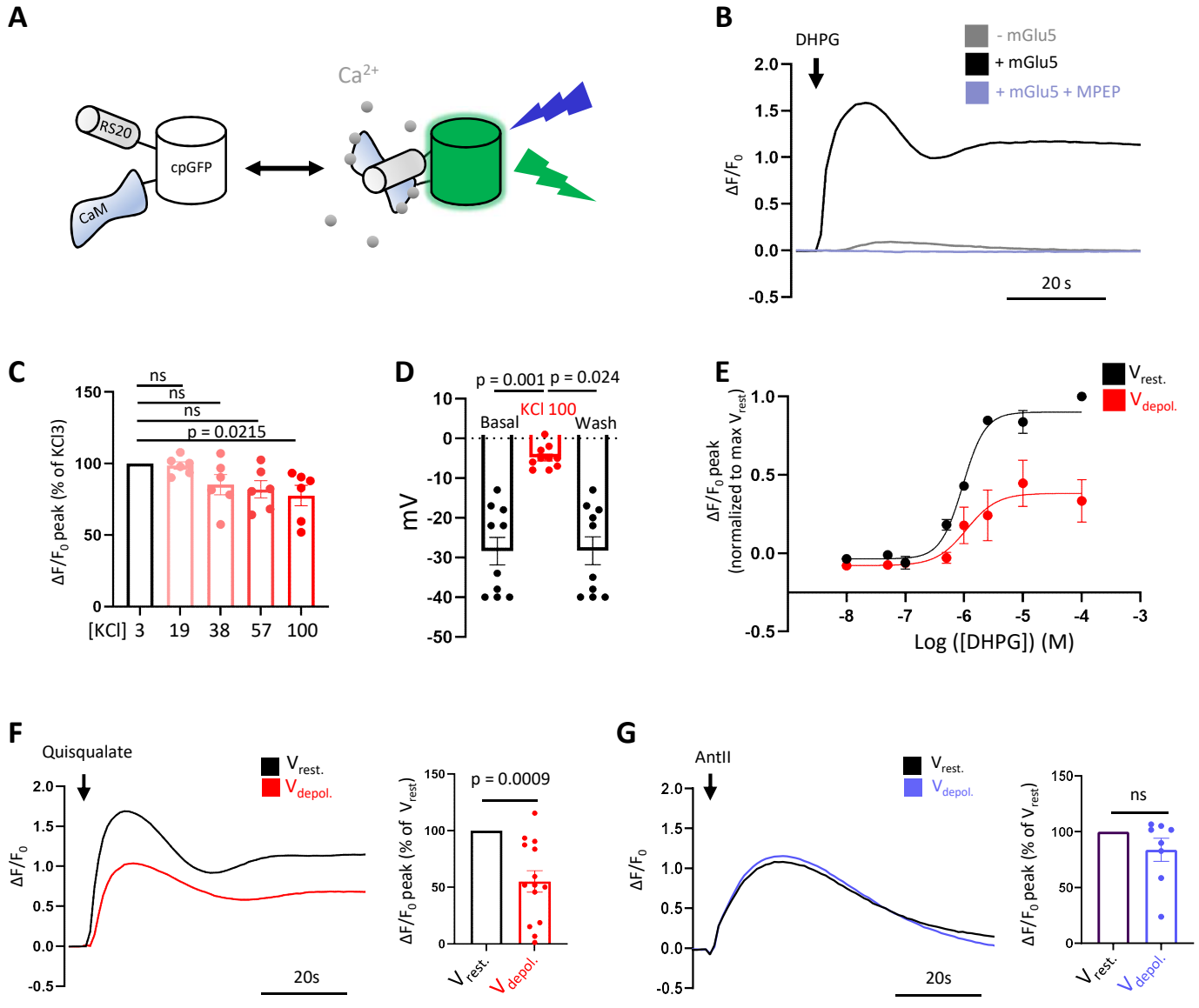
A
Ca2+
RS20
cpGFP
CaM
B
DHPG
- mGlu5
+ mGlu5
+ mGlu5 + MPEP
ΔF/F0
20 s
C
ns
ns
ns
p = 0.0215
ΔF/F0 peak (% of KCl3)
[KCl] 3 19 38 57 100
D
p = 0.001
p = 0.024
KCl 100
Basal
Wash
mV
E
Vrest.
Vdepol.
ΔF/F0 peak (normalized to max Vrest)
Log ([DHPG]) (M)
F
Quisqualate
Vrest.
Vdepol.
ΔF/F0
20s
p = 0.0009
ΔF/F0 peak (% of Vrest)
G
AntII
Vrest.
Vdepol.
ΔF/F0
20s
ns
ΔF/F0 peak (% of Vrest)

Figure 2

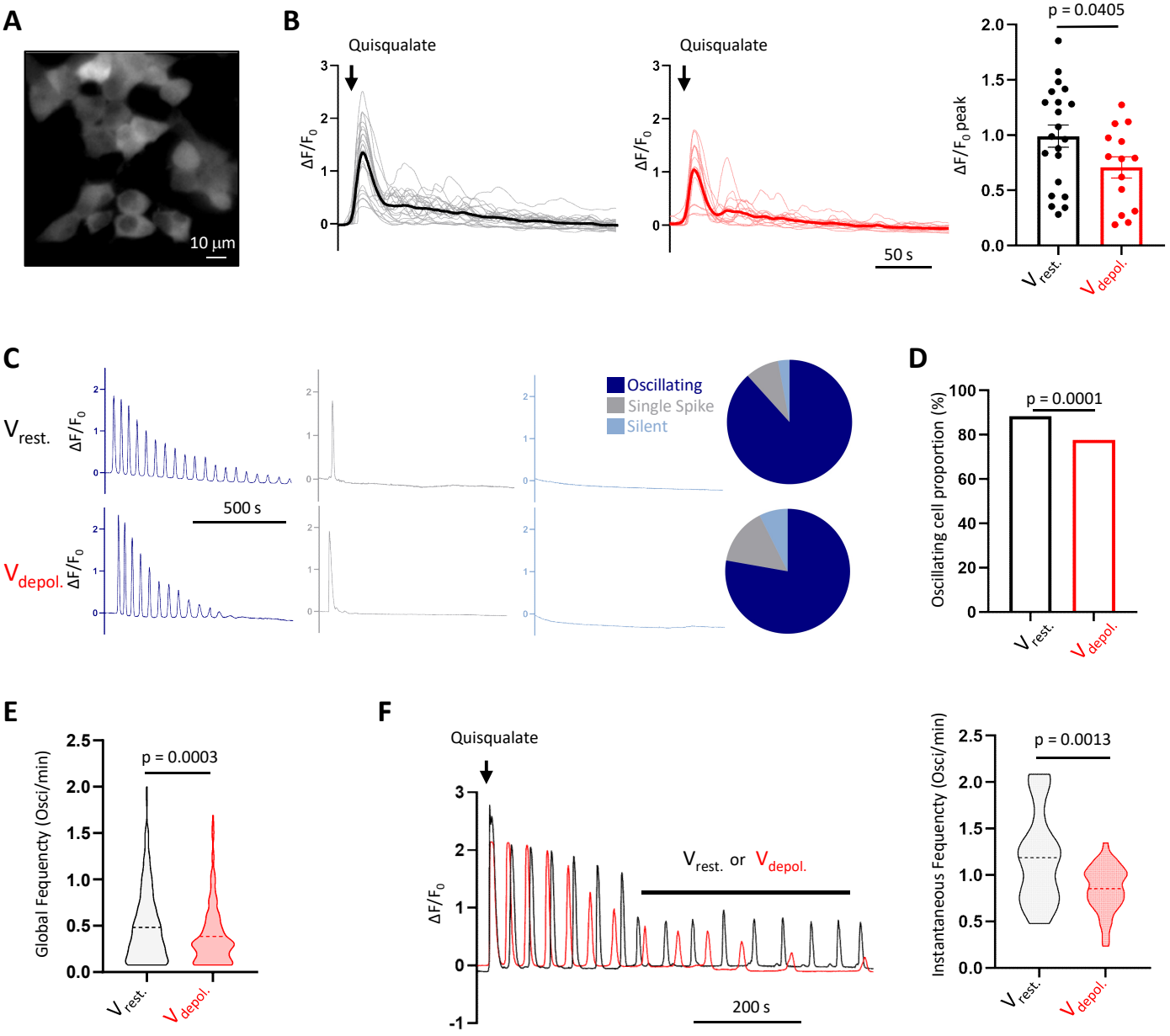
A
10 µm
B
Quisqualate
Quisqualate
ΔF/F0
50 s
p = 0.0405
ΔF/F0 peak
Vrest.
Vdepol.
C
Vrest.
Vdepol.
ΔF/F0
500 s
Oscillating
Single Spike
Silent
D
p = 0.0001
Oscillating cell proportion (%)
E
p = 0.0003
Global Fequencty (Osci/min)
F
Quisqualate
Vrest. or Vdepol.
200 s
p = 0.0013
Instantaneous Fequencty (Osci/min)

Figure 3

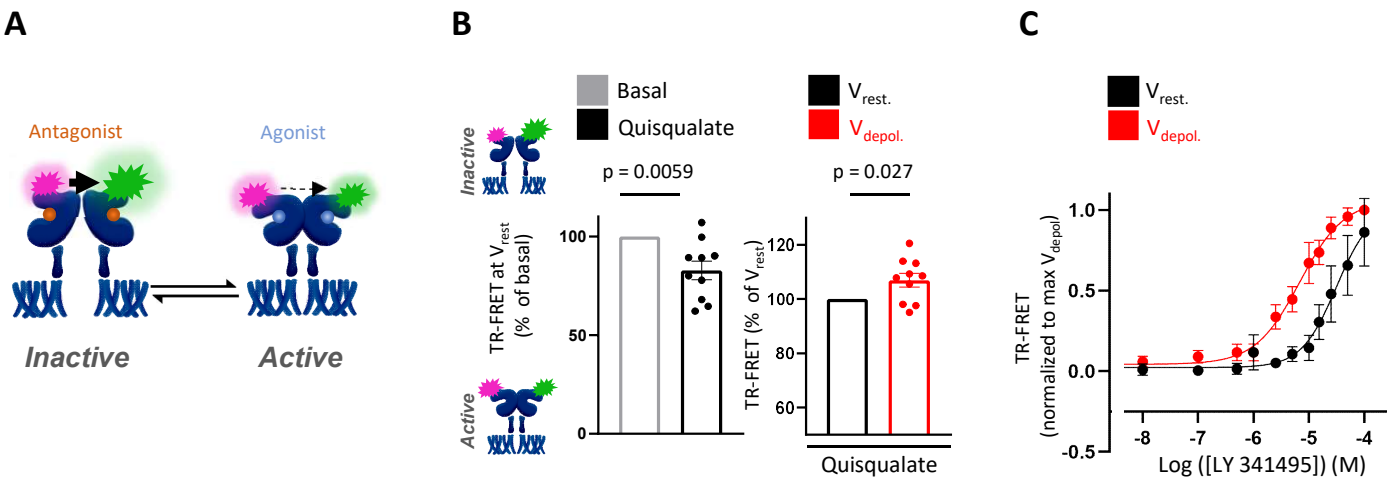
A
Antagonist
Agonist
Inactive
Active
B
Basal
Quisqualate
V rest.
V depol.
Inactive
Active
p = 0.0059
p = 0.027
TR-FRET at V rest (% of basal)
TR-FRET (% of V rest)
100
50
0
120
100
80
60
Quisqualate
C
V rest.
V depol.
TR-FRET (normalized to max V depol)
1.0
0.5
0.0
-0.5
-8
-7
-6
-5
-4
Log ([LY 341495]) (M)

Figure 4

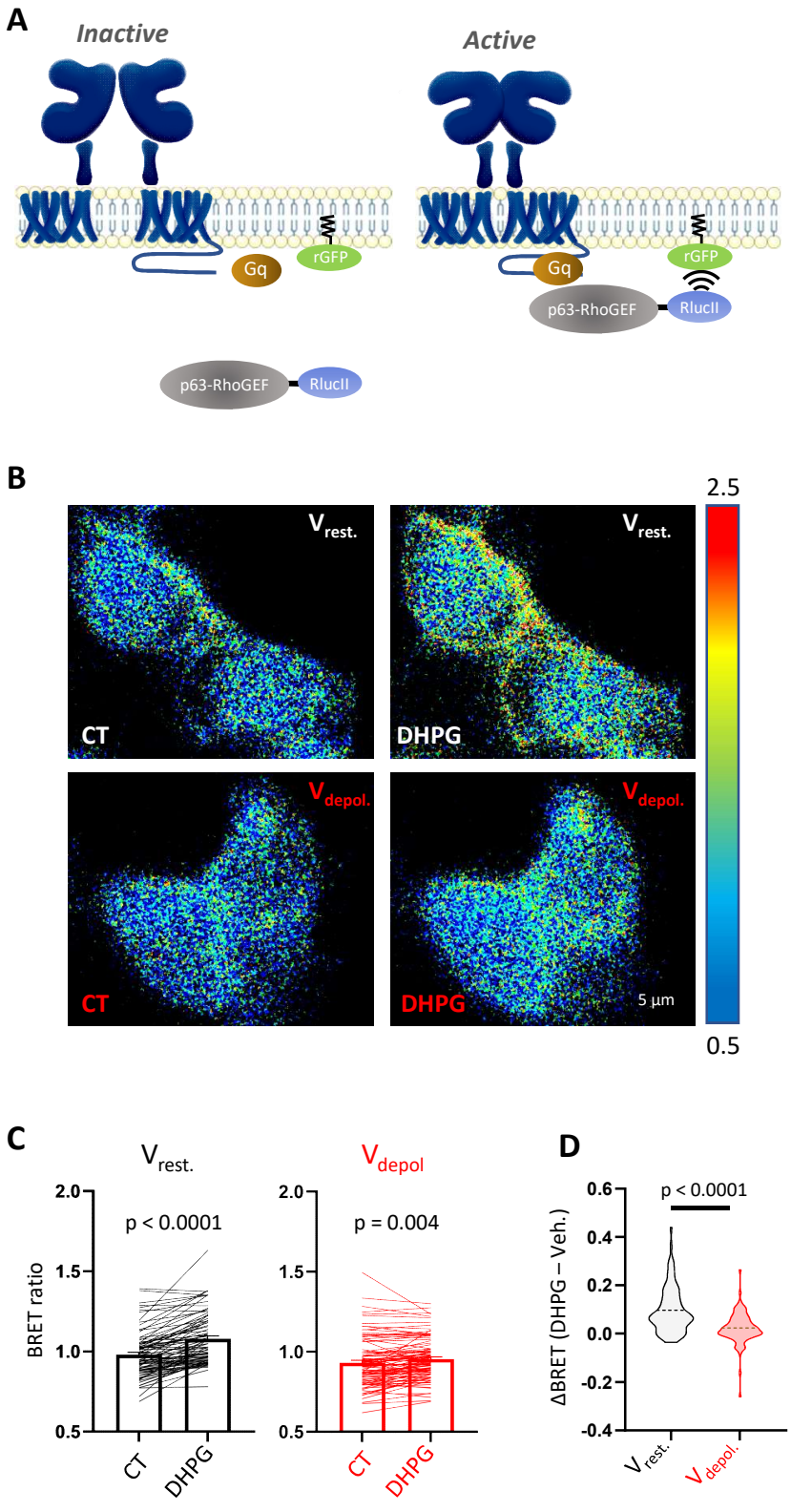
A
Inactive
Active
Gq
rGFP
p63-RhoGEF
RlucII
B
V rest.
CT
DHPG
V depol.
5 µm
2.5
0.5
C
V rest.
V depol
p < 0.0001
p = 0.004
BRET ratio
2.0
1.5
1.0
0.5
CT
DHPG
D
p < 0.0001
ΔBRET (DHPG – Veh.)
0.6
0.4
0.2
0.0
-0.2
-0.4
V rest.
V depol.

Figure 5

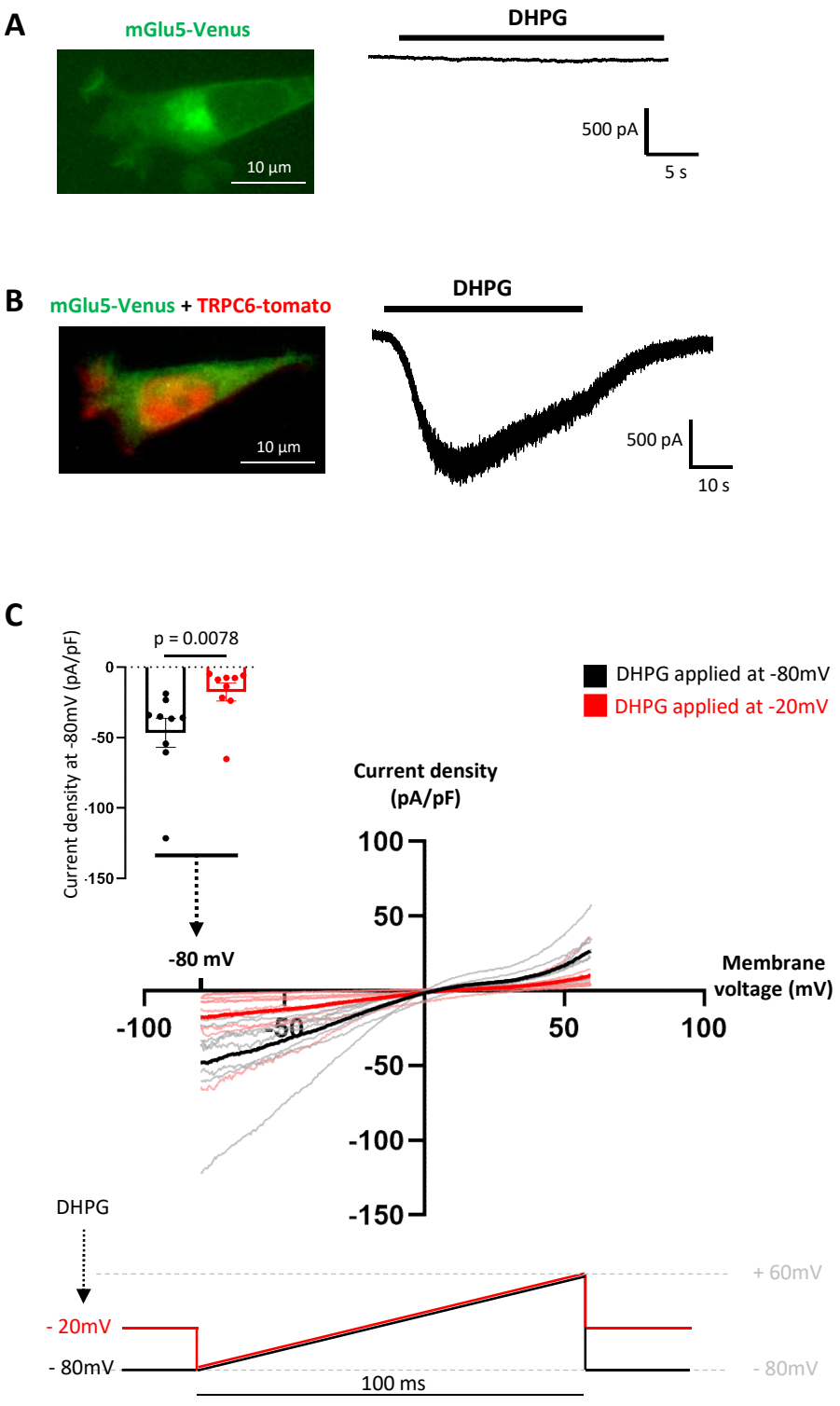
A
mGlu5-Venus
10 µm
DHPG
500 pA
5 s
B
mGlu5-Venus + TRPC6-tomato
10 µm
DHPG
500 pA
10 s
C
p = 0.0078
Current density at -80mV (pA/pF)
0
-50
-100
-150
DHPG applied at -80mV
DHPG applied at -20mV
Current density (pA/pF)
100
50
-50
-100
-150
-80 mV
-100
50
50
100
Membrane voltage (mV)
DHPG
+ 60mV
- 20mV
- 80mV
- 80mV
100 ms

Figure 6

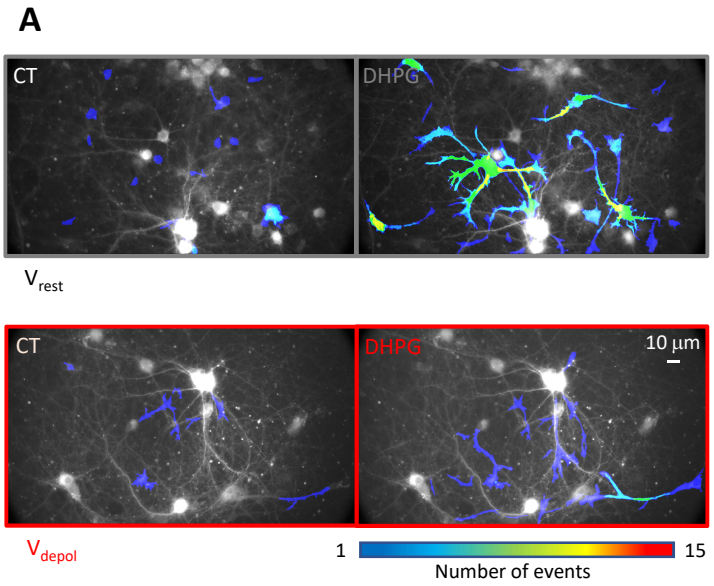
A
CT
DHPG
V rest
CT
DHPG
10 µm
V depol
1
15
Number of events
B
V rest CT
V rest DHPG
V depol CT
V depol DHPG
ΔF/F0
0.2
0.1
0.0
30 s
C
p = 0.03
Number of events
200
100
0
CT DHPG CT DHPG
V rest
V depol

Figure 7

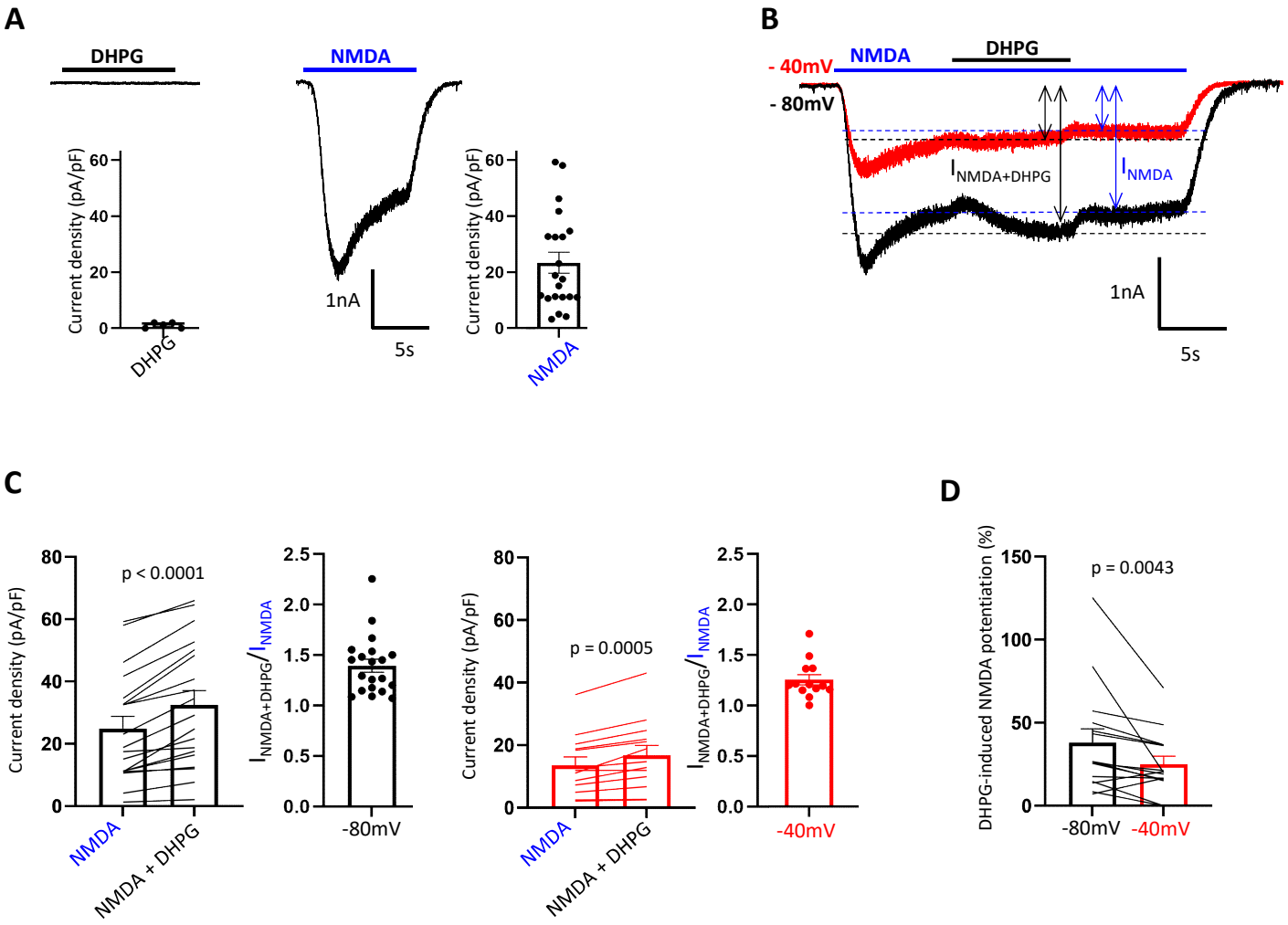
A
DHPG
NMDA
Current density (pA/pF)
60
40
20
0
DHPG
1nA
5s
Current density (pA/pF)
60
40
20
0
NMDA
B
- 40mV
- 80mV
NMDA
DHPG
I NMDA+DHPG
I NMDA
1nA
5s
C
Current density (pA/pF)
80
60
40
20
0
p < 0.0001
NMDA
NMDA + DHPG
I NMDA+DHPG / I NMDA
2.5
2.0
1.5
1.0
0.5
0.0
-80mV
Current density (pA/pF)
80
60
40
20
0
p = 0.0005
NMDA
NMDA + DHPG
I NMDA+DHPG / I NMDA
2.5
2.0
1.5
1.0
0.5
0.0
-40mV
D
DHPG-induced NMDA potentiation (%)
150
100
50
0
p = 0.0043
-80mV
-40mV

Figure 8

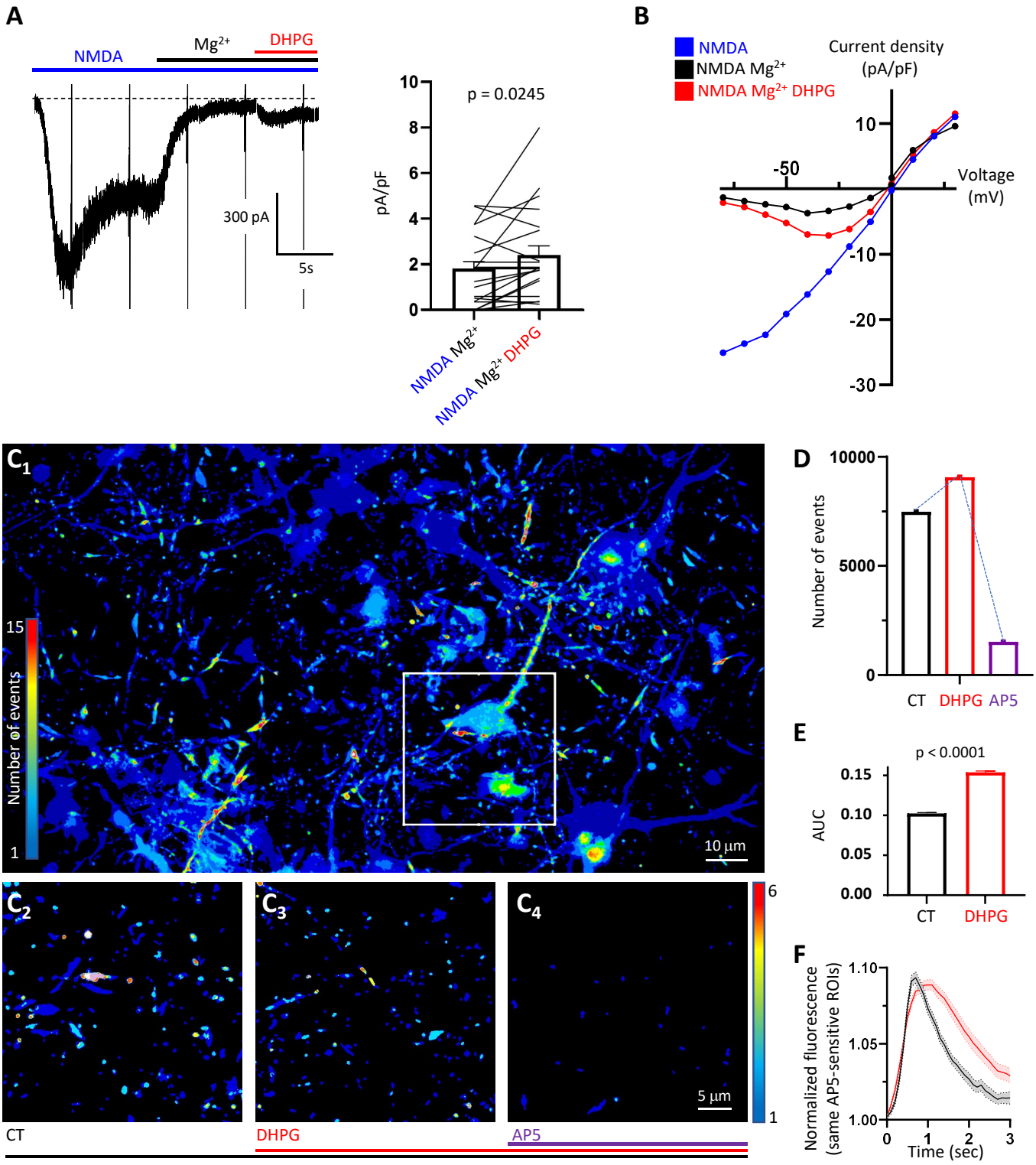
A
NMDA
Mg2+
DHPG
300 pA
5s
p = 0.0245
pA/pF
NMDA Mg2+
NMDA Mg2+ DHPG
B
NMDA
NMDA Mg2+
NMDA Mg2+ DHPG
Current density
(pA/pF)
Voltage
(mV)
C1
Number of events
10 µm
C2
C3
C4
5 µm
CT
DHPG
AP5
D
Number of events
CT DHPG AP5
E
p < 0.0001
AUC
CT DHPG
F
Normalized fluorescence
(same AP5-sensitive ROIs)
Time (sec)